ANNI JUNNILA
HUMAN INDUCED PLURIPOTENT STEM CELL DERIVED
CARDIOMYOCYTES GROWN ON WOVEN POLYETHYLENE
TEREPHTHALATE TEXTILE

Master of Science Thesis

ABSTRACT

ANNI JUNNILA: Human Induced Pluripotent Stem Cell Derived Cardiomyocytes Grown on Woven Polyethylene Terephthalate Textile
Tampere University of Technology
Master of Science Thesis, 71 pages, 7 Appendix pages
May 2016
Master's Degree Programme in Materials Science
Major: Polymers and Biomaterials
Examiners: Professor Minna Kellomäki and Master of Science Risto-Pekka Pölönen

Keywords: cardiomyocyte, human induced pluripotent stem cell, maturation, polyethylene terephthalate, textile

Cardiac tissue engineering aims to create functional tissue constructs in order to reestablish the function and structure of a damaged heart muscle using cells together with biomaterial scaffolds. One of the challenges is the cell source, because adult human cardiomyocytes (CMs) are difficult to obtain for study. However, CMs can be differentiated from pluripotent stem cells, one option being the human induced pluripotent stem cell (hiPSC). One of the main challenges in using hiPSC derived CMs (hiPSC-CMs) is that when cultured in normal *in vitro* conditions, they do not establish all the functional and morphological properties of adult CMs. The aim of this study was to produce structurally more mature hiPSC-CMs by culturing them on polyethylene terephthalate (PET) textiles.

The hiPSCs were differentiated into CMs by END-2 method. The resulted hiPSC-CMs were cultured on gelatin coated PET textiles for 11 days. Control hiPSC-CMs were cultured on gelatin coated coverslips. The primary analyzing methods used in this study were immunocytochemistry and fluorescence microscopy. The cells were labeled with antibodies against sarcomeric proteins and also with live/dead stainings. From immunostained images, hiPSC-CM's shape, multinucleation, and sarcomere organization, orientation and length were analyzed.

The structural maturation of hiPSC-CMs was evaluated by comparing cells cultured on PET textiles to the cells cultured on coverslips. Even though the amount of cells attached on the textiles was very small, it was found out, that the cells grown on textiles were more adult-like in shape, the sarcomeres were more organized, and the amount of multinucleated cells was higher. However, there was no significant difference in sarcomere lengths.

Based on the results, it can be argued that the cells grown on textiles were structurally more mature than the cells grown on coverslips. However, the small amount of cells attached on the textiles was a challenge. In future studies, the cell attachment should be improved, for example by using a different coating, in order to maintain more cells in the culture, thus making the analysis more reliable and reproducible.

TIIVISTELMÄ

ANNI JUNNILA: Ihmisen uudelleenohjelmoiduista kantasoluista erilaistettujen sydänlihassolujen kasvattaminen polyetyleenitereftalaattitekstiilillä
Tampereen teknillinen yliopisto
Diplomityö, 71 sivua, 7 liitesivua
Toukokuu 2016
Materiaalitekniikan diplomi-insinöörin tutkinto-ohjelma
Pääaine: Polymeerit ja biomateriaalit
Tarkastajat: professori Minna Kellomäki ja filosofian maisteri Risto-Pekka Pölönen

Avainsanat: sydänlihassolu, ihmisen uudelleenohjelmoitu kantasolu, kypsyminen polyetyleenitereftalaatti, tekstiili

Sydämen kudosteknologia tähtää vaurioituneen sydänlihaksen korjaamiseen soluista ja biomateriaaleista valmistetuilla funktionaalisilla kudosrakennelmilla. Yksi alan haasteista on solujen saatavuus, sillä aikuisen sydänlihassolujen hankkiminen tutkimustarkoituksiin on vaikeaa. Sydänlihassoluja voidaan kuitenkin erilaistaa pluripotenteista kantasoluista, kuten ihmisen uudelleen ohjelmoiduista kantasoluista (hiPS-soluista). Kun kantasoluista erilaistettuja sydänlihassoluja kasvatetaan *in vitro* -olosuhteissa, niiden käyttöön liittyy haasteita, sillä ne eivät saavuta kaikkia aikuisen sydänlihassolujen funktionaalisia ja morfologisia ominaisuuksia. Tämän tutkimuksen tavoitteena oli tuottaa rakenteellisesti kypsempiä, aikuisen sydänlihassolun kaltaisia hiPS-soluista erilaistettuja sydänlihassoluja kasvattamalla niitä polyetyleenitereftalaatista (PET) valmistetun tekstiilin päällä.

hiPS-solut erilaistettiin sydänlihassoluiksi END-2-menetelmällä. Näitä sydänlihassoluja kasvatettiin gelatiinilla pinnoitetuilla PET-tekstiileillä 11 päivän ajan. Kontrollinäytteinä käytettiin gelatiinilla pinnoitettujen peitinlasien päällä kasvatettuja hiPS-sydänsoluja. Ensisijaiset tutkimusmenetelmät olivat immunosytokemia ja fluoresenssimikroskopia. Immunovärjäyksillä saatiin visualisoitua sarkomeeriproteiineja, ja soluille tehtiin myös live/dead-värjäyksiä. Immunovärjätyistä kuvista analysoitiin solujen muotoa ja monitumaisuutta sekä sarkomeerien järjestäytyneisyyttä, orientaatiota ja pituutta.

hiPS-soluista erilaistettujen sydänlihassolujen rakenteellista kypsymistä arvioitiin vertaamalla tekstiileillä ja peitinlaseilla kasvatettuja soluja keskenään. Vaikka tekstiileille tarttuneiden solujen määrä oli vähäinen, havaittiin, että tekstiileillä kasvaneiden solujen muoto, sarkomeerien orientaatio ja monitumaisuus muistuttivat enemmän aikuisen sydänlihassoluja kuin peitinlaseilla kasvaneiden. Sen sijaan merkittävää eroa sarkomeerien pituuksissa ei havaittu.

Tulosten perusteella voidaan väittää, että tekstiileillä kasvatetut solut kehittyivät rakenteellisesti enemmän aikuisen sydänlihassolujen kaltaisiksi kuin solut, joita kasvatettiin peitinlaseilla. Tutkimuksen haasteena oli tekstiileille tarttuneiden solujen vähäinen määrä. Tulevaisuudessa solujen tarttumista tulisi parantaa esimerkiksi käyttämällä erilaista pinnoitetta, jotta enemmän soluja säilyisi viljelmässä ja analyyseistä tulisi luotettavampia ja toistettavampia.

PREFACE

Tampere 20.5.2016

Anni Junnila

CONTENTS

APPENDIX D: Reagents and Their Suppliers and/or Manufacturers

LIST OF FIGURES

LIST OF TABLES

LIST OF SYMBOLS AND ABBREVIATIONS

AV	atrioventricular
CM	cardiomyocyte
CVD	cardiovascular disease
DAPI	4', 6 diamidino-2-phenylindole
DNA	deoxyribonucleic acid
EB	embryoid body
ECM	extracellular matrix
END-2	mouse endodermal-like cell line
ESC	embryonic stem cell
GAPDH	Glyceraldehyde 3-phosphate dehydrogenase
hESC	human embryonic stem cell
hESC-CM	human embryonic stem cell-derived cardiomyocyte
hiPSC	human induced pluripotent stem cell
hiPSC-CM	human induced pluripotent stem cell-derived cardiomyocyte
hPSC-CMs	human pluripotent stem cell-derived cardiomyocyte
iPSC	induced pluripotent stem cell
iPSC-CM	induced pluripotent stem cell-derived cardiomyocyte
MEF	mouse embryonic fibroblast
MYBPC	myosin-binding protein C
NRVM	neonatal rat ventricular myocytes
Pa	Pascal
PCL	polycaprolactone
PDMS	polydimethylsiloxane
PEG	polyethylene glycol
PET	polyethylene terephthalate
PGA	polyglycolic acid
PLA	polylactic acid
PLGA	poly lactic-co-glycolic acid
PLLA	poly-L-lactic acid
PSC	pluripotent stem cell
PU	polyurethane
RNA	ribonucleic acid
SA	sinoatrial
SEM	scanning electron microscope

1. INTRODUCTION

Cardiac tissue engineering is a growing branch of research in the field of tissue engineering. One of the challenges in the research area has been the cell source of cardiomyocytes, because adult human cardiomyocytes (CMs) are difficult to obtain for study. An option is to use stem cells and differentiate them into cardiomyocytes. Human embryonic stem cells are pluripotent stem cells, which have the potential to differentiate into all human cells found in adults. However, certain technical and ethical problems limit the use of human embryonic stem cells as a cell source. (Chen et al. 2008; van Blitterswijk 2008, p. 7)

Another stem cell type capable of forming adult cell lines is the human induced pluripotent stem cell (hiPSC). These cells have been made by reprogramming adult human cells back into a pluripotent state. The advantages of hiPSCs include the lack of ethical problems associated with embryonic stem cells, as well as the production of patient and disease specific cells is possible. The hiPSC-CMs have the same genome as the donor. (Takahashi et al. 2007) This can be utilized in the field of cardiac tissue engineering, for example, for drug screening and disease modeling of inherited cardiac diseases (Khan et al. 2013).

One of the main challenges in using hiPSC derived cardiomyocytes (hiPSC-CMs) is that when cultured in normal *in vitro* conditions, they do not establish all the functional and morphological properties of adult CMs (Yang et al. 2014; Rao et al. 2013). Instead, their properties resemble more those of the human fetal CMs (Tzatzalos et al. 2016). The maturation of hiPSC-CMs is important for several reasons, including that mature cells would be more useful in drug screening and disease modeling, because they reflect the physiology of the adult CMs better. Also, in myocardial repair, the hiPSC-CMs introduced to the human body should have properties which resemble those of native cardiac muscle. (Yang et al. 2014)

This thesis concentrated on the structural maturation of hiPSC-CMs. While hiPSC-CMs are circular or irregularly shaped, the appearance of adult CMs is rectangular or rod-like, and adult CMs are significantly bigger than the hiPSC-CMs. Also, the smallest contractile units of CMs, sarcomeres, are disorganized in hiPSC-CMs, whereas the sarcomere structures in adult CMs are highly organized. (Yang et al. 2014)

The purpose of this thesis was to investigate whether the structural maturation of hiPSC-CMs could be enhanced by growing them on different PET textiles. The hypothesis was, that the cells would grow along the fibers of the textiles, and thus become more rod-like

in shape. Also, the sarcomere structures were expected to become more organized during the shape transition. The main tool for evaluating the maturation was staining the cells grown on PET textiles and imaging them using fluorescence microscopy.

2. LITERATURE REVIEW

2.1 Cardiac Tissue Engineering

Cardiovascular diseases (CVDs) are the leading cause of death worldwide. In 2012, approximately 31 % of all global deaths were caused by a CVD. (World Health Organization 2015) Due to this enormous clinical need, cardiac tissue engineering has become an important branch of research in the field of tissue engineering. The aim in cardiac tissue engineering is to create functional tissue constructs in order to reestablish the function and structure of a damaged heart muscle using stem cells and scaffolds made of biomaterials. (Chen et al. 2008; Vunjak-Novakovic et al. 2010)

The discovery and development of induced pluripotent stem cell (iPSC) technology has enabled the use of patient-specific stem cells for research. In the case of cardiac tissue engineering, iPSCs (which will be further discussed later) can be differentiated into spontaneously beating cells of the heart, cardiomyocytes (CMs). iPSC-derived cardiomyocytes (iPSC-CMs) can be characterized by various methods, and both healthy and disease-specific CMs can be produced. (Tzatzalos et al. 2016; Mummery et al. 2012) However, hiPSC-CMs cultured in normal *in vitro* conditions display immature phenotype (Rao et al. 2013).

In cardiac tissue engineering, CMs are often cultured on some kind of a biomaterial scaffold. The scaffold should mimic the functions of extracellular matrix (ECM) of CMs, at least partly. (Chen et al. 2008) For example, it should support cell attachment, growth, and differentiation, have sufficient mechanical properties, and provide porous structure for the diffusion of nutrients and metabolites (Chan & Leong 2008). Also, in the case of hiPSC-CMs, the use of biomaterials provide one possible approach to promoting hiPSC-CMs' maturation *in vitro*. Engineered heart tissue and iPSC-CM technologies are utilized, for example, for drug testing and disease modeling. Also, it is probable, that iPSC-CMs can be used as a tool for repairing the injured heart in the future. (Tzatzalos et al. 2016; Mummery et al. 2012)

The following subchapters include basics of cell culturing (Subchapter 2.1.1), a brief description of the human heart and cardiomyocytes (Subchapter 2.1.2), and an introduction to induced pluripotent stem cells (Subchapter 2.1.3) and human induced pluripotent stem cell derived cardiomyocytes (Subchapter 2.1.4). Biomaterials (Subchapter 2.2) and textiles as tissue engineering scaffolds (Subchapter 2.3) are discussed in their own sections after these topics. Also, a brief literature review of previous studies made by other research groups is included (Subchapter 2.4).

2.1.1 Cell Culturing

The general term for cell harvesting and the subsequent growth and maintenance of the cells in an artificial environment is a cell culture. When cultured *in vitro*, cells have the same basic needs as cells grown within an organism, for example the human body. (Ratner et al. 2013, p. 408) In the human body, blood is responsible for carrying nutrients and waste products. In a cell culturing system, the nutrients are introduced to the cells via cell culture medium, which is an *in vitro* substitute for a biological fluid. (van Blitterswijk 2008, pp. 328–329) In addition to nutrients (salts and amino acids), cell culture medium contains proteins and hormones (from added serum), a buffer (maintains pH balance), and an energy source (glucose). The byproducts of cellular metabolism are released into the medium as the cells are depleting medium's ingredients. Thus, the culture medium must be changed regularly to maintain the optimal conditions. (Ratner et al. 2013, p. 408)

Cell culturing systems are often categorized in static and dynamic systems. In static systems, the culture is not exposed to external forces, and the only effects are caused by interaction with the environment and by conduction and reaction processes within the system. By contrast, in dynamic cell culture systems, there are external forces involved. The system can have a mechanical, hydraulic, or pneumatic power input. (Eibl et al. 2009, p. 57) Different static cell culturing systems are illustrated in Figure 2.1. In order to enhance the ability of cell binding to the cell culture substrate, different kinds of coatings, for example gelatin or collagen, are often applied to the surfaces (van Blitterswijk 2008, p. 316).
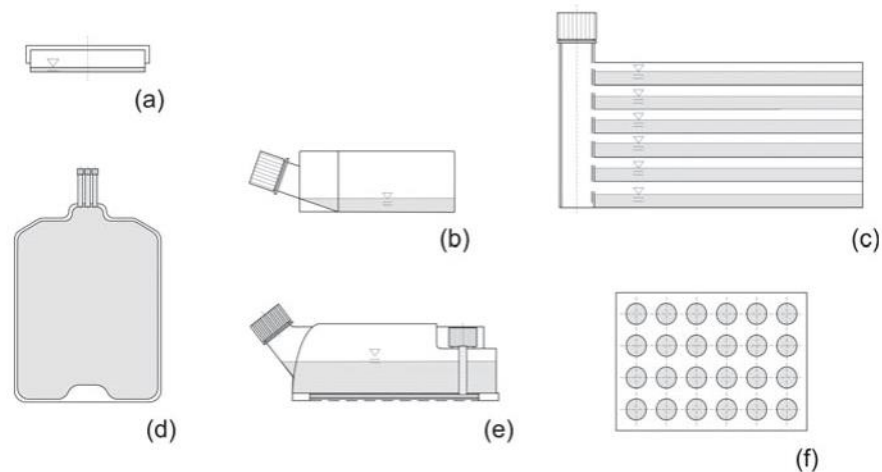
Figure 2.1. Different static cell culture systems with unenforced power input: (a) Petri dish, (b) T-flask, (c) multitray cell culture system, (d) culture bag, (e) static membrane flask bioreactor, and (f) multiwell plate. (Eibl et al. 2009, p. 59)

Cell culture systems are incubated in a chamber, which is temperature-controlled and humidified. The temperature is kept at the temperature of the human body (37 °C), and the humidity is approximately 95 %. Also, carbon dioxide (CO_2) is added to the incubator at a low concentration (5 %). CO_2 helps maintain a pH of 7.0–7.4 by interacting with the

buffer in the culture medium. Since these culture conditions are also favorable for unwanted organisms (fungi, bacteria) to grow, contaminations are avoided by handling cells under a laminar hood using strict sterile methods. Also, anti-fungal and anti-bacterial substances are often added to the cell culture medium. (Ratner et al. 2013, pp. 408–409)

In the human body, many organs have different cell types that act together as a team supporting each other. In some cases, the same idea is used in cell cultures *in vitro*: cells are co-cultured with another cell type. In co-cultures, so-called feeder cells are first seeded on a cell culturing system, e.g. Petri dish. Feeder cells are supporting cells from a rapidly growing cell line, for example a mouse cell line. When the Petri dish reaches the desired confluence, the cell proliferation is arrested by irradiation or by treating the cells with a mitosis arresting drug, Mitomycin. After that, the cells of interest can be seeded on top of the feeder cells. Feeder cells have many functions: processing of nutrients, detoxification, activation and deactivation of hormones and growth factors, and also acting as a supporting cell matrix. (van Blitterswijk 2008, p. 317)

Feeder cells can be utilized, for example, in stem cell cultures, in which the feeder cells allow the continuous growth of stem cells while maintaining their undifferentiated state. Feeder cells provide nutrients and a surface to which the stem cells can attach. When not cultured on feeder cells, stem cells require a matrix for attachment and growth. (Amit et al. 2003) Feeder cells are also utilized in producing other cell types from stem cells. For example, hiPSCs can be differentiated into CMs by co-culturing them with mouse endodermal-like (END-2) cells, which secrete differentiation inducing factors into the culture medium. (Mummery et al. 2003; Passier et al. 2005)

2.1.2 The Heart and Cardiomyocytes

The primary task of the heart is to maintain blood pressure and circulation. In order to carry out this task properly, the heart muscle is specialized to produce a coordinated and rhythmic contraction. The heart receives oxygen-poor blood that returns from the tissues of the body via the venous circulation. The oxygen-poor blood is then sent to the lungs for oxygenation. Also, the heart must receive the oxygenated blood and send that blood via the arterial circulation to the rest of the body. This process of coordinated pumping of blood requires precise timing of the contractions of the four chambers of the human heart. (Matthews 2009, p. 191)

The walls of a chamber consists of three layers: peri-, myo- and endocardium. Myocardium, the heart muscle, consists of cardiomyocytes and connective tissue. Cardiomyocytes contain dozens of parallel cylindrical elements, myofibrils. Each of these comprises repeating units, sarcomeres (Figure 2.2). (Sparrow & Schöck 2009; Boron & Boulpaep 2005, p. 232)
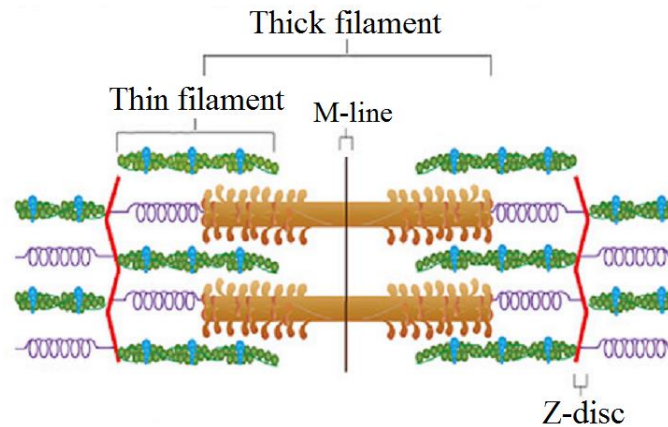
Figure 2.2. Sarcomere structure, adapted from (Pasqualini et al. 2015). A sarcomere is bordered by two Z-discs, and it consists of myosin-containing thick filaments and actin-containing thin filaments. The thick filaments are anchored at the M-line, which lies half way between the Z-discs.

A sarcomere is the smallest functional contractile unit of a muscle, and it consists of two types of myofilaments: myosin-containing thick filaments and actin-containing thin filaments. The thick filaments are anchored at the M-line and they lie between the thin filaments. Myofibrils are made up by stacking sarcomeres end to end and they have the diameter of a Z-disc. One sarcomere is bordered by two Z-discs, which the sarcomere shares with its neighboring sarcomeres. (Sparrow & Schöck 2009; Boron & Boulpaep 2005, pp. 232–233) In adult cardiomyocytes, the sarcomere structures are highly organized, as seen in Figure 2.3. Also, the cells are rod-shaped or cylindrical, and they may contain multiple nuclei. (Robertson et al. 2013; Yang et al. 2014)
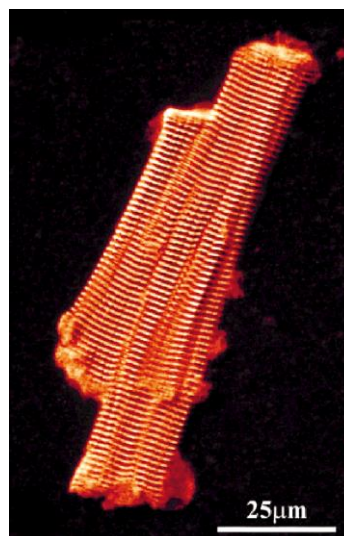
Figure 2.3. Confocal microscopy image of single adult cardiomyocyte, adapted from (Severs 2000). The image shows myofibrils, which are seen as striations. The myofibrils are revealed by immunostaining with an antibody against α-actinin, a component found in the sarcomere Z-discs.

In the cardiac muscle contraction, the atria and the ventricles contract one after another. The electrical signals that trigger the cardiac muscle contraction originate in the pacemaker region of the heart, the sinoatrial (SA) node, which generates action potentials spontaneously and periodically. The SA node is located in the wall of the right atrium, and it sends action potentials to the cardiomyocytes of the right and left atria, making them contract. The excitation spreads and reaches the atrioventricular (AV) node, which is located in the lower part of the right atrium. From the AV node, the excitation propagates fast through the rest of the conducting system: the bundle of His, the right and left bundle branches, and finally, the Purkinje fibers, which transmit the action potentials to the cardiomyocytes of the ventricles. (Schmidt & Thews 2013, p. 360; Anna 2011, p. 93) The electrical conduction system of the heart is illustrated in Figure 2.4.
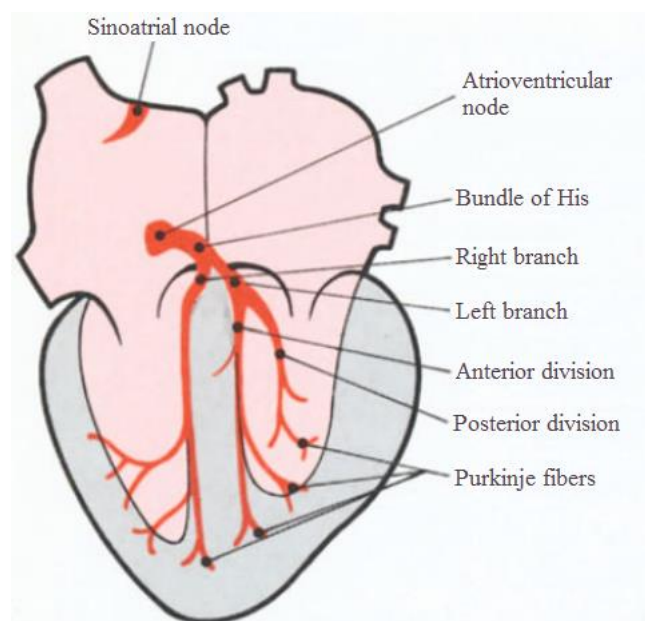
Figure 2.4. Electrical conduction system of the heart as seen in frontal section, adapted from (Schmidt & Thews 2013, p. 360).

Cardiomyocytes must contract at the same time in order to pump blood. In cardiac muscle, the excitation spreads rapidly out from one cell to another, which enables the cardiomyocytes to contract simultaneously. The rapid spreading is enabled by specialized structures called intercalated discs. The process from electrical excitation of a cardiomyocyte to contraction of the cardiac muscle is called cardiac excitation-contraction coupling. The underlying trigger for muscle contraction is a rise in the free intracellular Ca^{2+} concentration $[Ca^{2+}]_i$, which is briefly explained in the following paragraph. (Bers 2002; Matthews 2009, p. 193; Boron & Boulpaep 2005, p. 522)

During heart muscle contraction, the thick filaments establish cross-bridges to the thin filaments. The making and breaking of cross-bridges results in drawing the thin filaments over the thick filaments, which causes the muscle contraction. As the action potential travels, it activates Ca^{2+} channels which allow the Ca^{2+} ions to enter the cell. The entry of

the Ca^{2+} ions triggers Ca^{2+} ion release from the sarcoplasmic reticulum, an organelle which functions as a storage for intracellular Ca^{2+} ions. Because of the Ca^{2+} influx and release, the free intracellular $[Ca^{2+}]_i$ rises, after which the Ca^{2+} ions are able to bind to the thin filament protein troponin C. This allows the thick filament to form cross-bridges to the thin filament. Relaxation occurs when $[Ca^{2+}]_i$ decreases and Ca^{2+} ions dissociate from troponin. (Bers 2002; de Tombe 2003)

2.1.3 Induced Pluripotent Stem Cells

Stem cells are cells, which have the ability to produce new stem cells (self-renewal) and any other cell type of the body (differentiation). A term "potency" defines the differentiation capacity of a stem cell. The used terms are totipotent, pluripotent, multipotent, oligopotent and unipotent stem cells. Totipotent stem cells are able to form an entire organism. The cells that are considered totipotent, are the fertilized oocyte and the cells that are formed in the first cleavage divisions. Pluripotent stem cells can form all three germ layers (ectoderm, mesoderm and endoderm) including germ cells. However, pluripotent stem cells (PSCs) are not able to form extra-embryonic tissue (e.g. placenta). Pluripotent cells are found in the blastocyst, and when brought into a cell culture, they are referred to as embryonic stem cells (ESCs). Multipotent stem cells are able to form multiple cell types. For example, mesenchymal stem cells have the ability to differentiate into bone, cartilage and adipose cells. Oligopotent stem cells are able to form two or more lineages. For instance, neural stem cells, which can differentiate into a subset of neurons in the brain, are oligopotent stem cells. Lastly, unipotent stem cells can form cells from a single lineage. (van Blitterswijk 2008, p. 3)

Even though human embryonic stem cells (hESCs) are a promising cell source for disease and injury treatments, there are still some problems in their use in patients. Technical problems include immune rejection of transplanted hESCs, and there are also ethical problems in the use of human embryos as a cell source. (van Blitterswijk 2008, p. 7) In order to isolate hESCs, the human blastocyst has to be destructed, and that is an issue which has induced multiple debates concerning the ethics of hESC derivation. Also, regulations concerning the usage and research of hESCs have been set across the world. In the European Union, the Court of Justice forbade the patenting of any process involving the destruction of human blastocyst in 2011. The regulation has caused concern for the scientific community because the investors might lose interest in the research using hESCs. (de Lázaro et al. 2014) The technical and ethical problems, among others, led scientists to seek for other possibilities (van Blitterswijk 2008, p. 7).

Induced pluripotent stem cells (iPSCs) were found by Shinya Yamanaka and collaborators who published the study in 2006. Yamanaka's group was able to turn mouse fibroblasts back into a pluripotent state, and the resulting cells were called iPS cells. The results were achieved by genetically reprogramming fibroblasts by retroviral transduction of four transcription factors which are needed for the maintenance of embryonic stem

cells' pluripotency. The four transcription factors were Oct-3/4, Sox2, c-Myc and Klf-4. (Takahashi & Yamanaka 2006) In 2007, Yamanaka's research group published a study, where a similar approach was succesfully applied to human dermal fibroblasts. The study showed that human induced pluripotent stem cells (hiPSCs) can be generated by retroviral transduction of the same four transcription factors that were used in the generation of mouse iPSCs. (Takahashi et al. 2007). Also, a contemporaneous study accomplished the same result by using a different combination of transcription factors: OCT4, SOX2, NANOG, and LIN28 (Yu et al. 2007).

At first, scientists were amazed by how remarkably similar iPSCs and ESCs were. After further studies, however, conflicting conclusions regarding the similarity of these cells were made. For example, some studies demonstrated that iPSC clones and ESC clones are difficult to distinguish and that their gene expression and DNA methylation are very similar – some studies concluded the opposite. In addition, different studies regarding the differentiation efficacy of iPSCs compared to that of ESCs reported different results. However, different properties of iPSCs produced in different laboratories depend on technical variables, such as different gene delivery methods and different laboratory culture conditions. Also, some differencies can be explained by uncontrollable stochastic events during reprogramming. (Yamanaka 2012; Bilic & Belmonte 2012)

2.1.4 Human Induced Pluripotent Stem Cell Derived Cardiomyocytes

Many laboratories have successfully differentiated hiPSCs to cardiomyocytes. These hiPSC derived cardiomyocytes (hiPSC-CMs) beat spontaneously in cell culture. They exhibit functional properties similar to the cardiomyocytes in the developing heart, and express ion channels and sarcomeric proteins which are expected from cardiomyocytes. (Yang et al. 2014) Cardiomyocytes can be differentiated from hiPSCs in several ways. For example, one option is a spontaneous differentiation of hiPSCs in embryoid bodies (EBs). EBs are three-dimensional multicellular aggregates formed by hiPSCs. The method is relatively simple and inexpensive, but the differentiation rate is low. Only a small part of the EBs form spontaneously beating areas. Also, cardiac differentiation can be achieved using defined growth factors. The idea is to activate or stimulate the signaling pathways which are responsible for cardiac differentiation during embryonic development *in vivo*. (Kujala et al. 2011; Kurosawa 2007; Acimovic et al. 2014) Yet another method is to co-culture hiPSCs with mouse endodermal-like (END-2) cells, in which the END-2 cells secrete differentiation inducing factors into the culture medium. (Mummery et al. 2003; Passier et al. 2005)

hiPSC-CMs enable the use of patient specific cells: the CMs are derived from iPSCs, which in turn are produced from the patient's own cells (e.g. fibroblasts). Thus, the hiPSC-CMs have the same genome as the patient. This can be utilized in cardiac tissue

engineering, since the hiPSC-CMs produced from a patient with inherited cardiac disease carry the same genetic mutation as the patient itself. These patient specific hiPSC-CMs have many applications. They can be used in drug screening, disease modeling, and hopefully in patient targeted cell therapy in the future. Also, hiPSC-CMs are a potentially unlimited source of human cardiomyocytes. (Khan et al. 2013) The problem in using hiPSC-CMs is that they do not exhibit all the functional and morphological characteristics of adult CMs when grown in normal 2-dimensional *in vitro* culture conditions (Yang et al. 2014; Rao et al. 2013). Instead, hiPSC-CMs' gene expression, structural, and functional properties resemble more those of the human fetal CMs (Tzatzalos et al. 2016).

There are many ways to evaluate the maturation of hiPSC-CMs. Firstly, cell morphology can be compared to that of adult CMs. For instance, shape and size, sarcomere alignment and cell-to-cell alignment can be compared. Secondly, functional assays can be used to study, for example, calcium transients, contraction, and electrophysiology of the cells. Finally, molecular assays can be utilized in gene expression analysis. (Tzatzalos et al. 2016) This study will concentrate on the morphological maturation of hiPSC-CMs. Some morphological differences between hiPSC-CMs and adult CMs are given in Table 2.1.

Table 2.1. *Morphological differences between hiPSC-CMs and adult cardiomyocytes (Yang et al. 2014; Mummery et al. 2012; Robertson et al. 2013).*

Parameters	hiPSC-CMs	Adult CMs
Cell shape	Circular, irregular	Rod-shaped, rectangular
Cell size	Small (≈ 300 μm^2)	Large (≈ 1500 μm^2)
Sarcomere structure	Disarrayed	Highly organized
Sarcomere length	≈ 1.6 μm	≈ 2.2 μm
Multinucleation	Mononucleated	≈ 25 % multinucleated

As seen in Table 2.1, hiPSC-CMs differ from adult CMs in cell shape and size, sarcomere structure and length and in the number of nuclei. hiPSC-CMs are circular and irregularly shaped, whereas adult CMs are rod-shaped. Also, hiPSC-CMs are significantly smaller than adult CMs. According to Robertson et al. (2013), adult CMs can be 150×10 μm, whereas hiPSC-CMs are usually 30×10 μm at most. The sarcomere structures in hiPSC-CMs are disarrayed and the sarcomere length is approximately 1.6 μm. By contrast, in adult CMs they are highly organized and the sarcomeres are longer, approximately 2.2 μm m. (Robertson et al. 2013; Yang et al. 2014; Mummery et al. 2012)

The studies regarding multinucleation of CMs are not unanimous, and it is not clear whether the multinucleation of CMs is a maturation marker or not. According to

Robertson et al. (2013), hiPSC-CMs are mononucleated, whereas most adult CMs have multiple nuclei. Another source claims that the estimated percentage of binucleation of mature CMs is 25 %, which is reached a few months after birth (Yang et al. 2014). In contrary, some sources state that fully differentiated CMs only have a single nucleus (Sparrow & Schöck 2009).

There are several reasons why the maturation of hiPSC-CMs is important. Firstly, adult human cardiomyocytes are difficult to obtain for study. Secondly, mature cells would be more useful in disease modeling and drug screening, since they reflect the physiology of the adult CMs better. Finally, when introducing cells into the human body in myocardial repair, hiPSC-CMs should have electric and mechanical properties which resemble the properties of native cardiac muscle. Mature cardiomyocytes would expectedly have enhanced contractile performance. Also, there should be a smaller risk of arrhythmia. (Yang et al. 2014)

2.2   Biomaterials

The definition of a biomaterial was given by The National Institutes of Health Consensus Development Conference, which defined a biomaterial as "any substance (other than a drug) or combination of substances, synthetic or natural in origin, which can be used for any period of time, as a whole or as a part of a system which treats, augments, or replaces any tissue, organ, or function of the body" (Boretos & Eden 1984, pp. 232–233). In other words, a biomaterial is a material which is able to exist and perform in contact with living tissues or tissue components without causing an unacceptable amount of harm to them. This ability of a biomaterial is often referred to as biocompatibility. (van Blitterswijk 2008, p. 256) The Williams Dictionary of Biomaterials (Williams 1999, p. 40) defines biocompatibility as "the ability of a material to perform with an appropriate host response in a specific application."

Biomaterials are found in all material classes: metals, polymers, ceramics, and composites. Also, biomaterials can be classified into different types, for example bioactive, biostable, and biodegradable. Bioactive materials promote the bonding of a living tissue to the material. (Patel & Gohil 2012; Dee et al. 2002) Biostable materials are able to resist structural and chemical degradation within a biological environment. In practice, all materials are subjected to some changes when placed in a biological environment. The term biostable refers to situations, where the changes have no clinical consequences. (Williams 1999, p. 44) Biodegradable materials degrade and are replaced by regenerated tissue when placed in the human body (Dee et al. 2002).

Polymers are the most used material class in the biomedical field because of their many unique properties, such as high porosity with a very small pore size and high surface-to-volume ratio. The main types of polymers used as biomaterials are naturally occurring polymers, synthetic biodegradable, and synthetic biostable polymers. Naturally occurring

polymers include proteins (gelatin, collagen), polysaccharides (cellulose, chitin), and polynucleotides (DNA, RNA). Naturally occurring polymers have bioactive properties. Also, they can be considered as the first clinically used biodegradable materials. However, synthetic polymers have many advantages over naturally occurring polymers. For example, their properties, such as mechanical characteristics, porosity, and degradation time, can be tailored for different applications. In addition, they are often cheaper, they can be produced in large quantities, and their shelf time is longer. (Dhandayuthapani et al. 2011) Biodegradable polymers can be classified into hydrolytically and enzymatically degradable polymers, since the biodegradation of polymeric biomaterials occurs via cleavage of hydrolytically or enzymatically sensitive bonds. Due to their minimal patient-to-patient and site-to-site variations, hydrolytically degradable polymers are usually more favorable as implants compared to enzymatically degradable polymers. (Nair & Laurencin 2007)

In tissue engineering applications, biodegradable polymers are often more favorable than biostable polymers, because many permanent implants have long-term biocompatibility issues. Also, there is no need for a second surgery when using biodegradable materials. (Nair & Laurencin 2007) However, it should be mentioned that biocompatibility issues exist with biodegradable materials, too. The problems include pro-inflammatory products released during the degradation process. Thus, in the cases where it is acceptable for the material residue to remain in the body after the tissue regeneration, biostable materials can be considered as one option for the application. (van Blitterswijk 2008, p. 269) Some biostable polymers, such as polyethylene terephthalate (PET), have been investigated also for cardiac tissue engineering. One typical application is cardiovascular grafting. (Chen et al. 2008)

2.3   Textiles as Tissue Engineering Scaffolds

Textile materials can be produced in many different forms, including woven, nonwoven, and knitted fabrics, and monofilament and multifilament yarns. Unlike many other polymeric materials, textiles offer compliance and porosity within the material structure, and they can meet the needs of applications, which require a combination of flexibility, strength, and in some cases moisture and air permeability. Because of their ability to form a wide range of different kinds of structures with different kinds of properties, textile materials are an especially attractive option for the production of tissue engineering scaffolds. (Alagirusamy & Das 2010, pp. 452–453)

In addition to biocompatibility, two important aspects of scaffold design are the mechanical and microstructural properties, both of which can be tailored by using different textile techniques (Tao 2001, p. 298). In this study, cardiomyocytes were cultured on woven textile structures. Thus, some microstructural and mechanical properties of scaffolds made by weaving are given in Table 2.2. The weaving process is further discussed later.

Table 2.2. Microstructural and mechanical properties of woven textile scaffolds (Tao 2001, p. 300; 304).

Microstructural		Mechanical	
Pore size (µm)	0.5−1000	**Stiffness**	High
Porosity (%)	30−90	**Strength**	High
Pore distribution	Uniform	**Structural stability**	Excellent
Pore connectivity	Excellent	**Isotropy**	Anisotropic (properties depend on direction of measurement)

The optimum design of a scaffold depends on which kind of a tissue it is prepared for. Ideally, the mechanical properties of a scaffold should match those of the surrounding tissues, but the scaffold must also be strong enough to withstand surgical handling during implantation. The microstructural properties include porosity, pore size and distribution, and pore interconnectivity. For example, cellular penetration and diffusion of nutrients and waste products depend on these factors. (Tao 2001, p. 298; O'Brien 2011)

Textiles as tissue engineering scaffolds have been studied for many applications. For example, Karamuk et al. (1999) studied woven PET textile scaffolds coated with thin poly lactic-co-glycolic acid (PLGA) film for liver cell culture. The fiber diameters were not mentioned in the article, but the mesh sizes varied from 50 µm to 800 µm. It was found out, that the mesh size of the textiles had an effect on hepatocytes' aggregation behavior. On large meshes, the hepatocyte aggregation required 48 hours, whereas on smaller meshes it required four days. The pores of the textiles were filled with aggregates, which showed the possibility of immobilizing hepatocyte aggregates on periodical textile structures.

In another study, Zong et al. (2005) investigated biodegradable nonwoven electrospun PLGA-based scaffolds for heart tissue constructs. The fiber diameters were approximately 1 µm, and the fibers were randomly oriented. The electrospun scaffolds were post-processed by uniaxial stretching in order to improve the fiber alignment. It was found out, that the oriented fiber structure promoted anisotropic cell growth along the stretching direction.

Moreno et al. (2011) developed micro-fibrous nonwoven PET scaffolds for vascular grafting. Scaffolds with different fiber diameters and pore sizes were produced. The most suitable scaffold for culturing endothelial cells and smooth muscle cells was the one having the smallest diameter range (from 1 µm to 5 µm) and pore size range (from 1 µm

to 20 μm). The proposed reason was that the cells were more easily trapped in the smaller pores when seeding the cells.

In addition, Ebersole et al. (2012) evaluated the suitability of electrospun nonwoven polycaprolactone (PCL) scaffolds for hernia repair. Six different scaffolds were produced by changing the polymer concentration and flow rate in electrospinning. The fibers were randomly oriented, and the fiber diameters ranged from 1.0 ± 0.1 μm to 1.5 ± 0.2 μm. Two of the six electrospun scaffolds (polymer concentration 12 %, flow rates 10 mL/h and 6 mL/h) were found to have appropriate mechanical properties for hernia repair.

2.3.1 Polyethylene Terephthalate

Polyethylene terephthalate (PET) belongs to the family of the engineering polyesters, and it is a basic material used in the textile industry. Polyester and PET are often used as synonyms, even though other polyesters (such as polybutylene terephthalate) exist, too. Because of its high crystallinity and hydrophobicity, PET is relatively stable *in vivo*, and it is considered to be a biostable material. (McKeen 2010, p. 100; Hu & Yang 2000; Ratner et al. 2013, p. 700; Ebnesajjad 2013, pp. 94–95)

Polyesters contain characteristic ester groups in the polymer backbone and they are usually prepared by reacting a dibasic acid with a dihydric alcohol. The reaction is shown in Figure 2.5, where X and Y present aromatic or alkyl units. (Hu & Yang 2000)

$$\text{HOOC-X-COOH} + \text{HO-Y-OH} \longrightarrow \text{--OC-X-COO-Y-O --- } + H_2O$$
Dibasic acid   Dihydric alcohol   Polyester
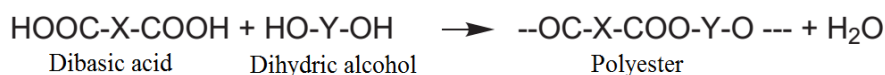
Figure 2.5. Reaction between a dibasic acid and a dihydric alcohol in polyester preparation, adapted from (Hu & Yang 2000).

For polyethylene terephthalate, the X and the Y in the equation represent a 1,4-phenylene ring and ethylene, respectively. PET is formed in a polycondensation reaction between terephthalic acid and ethylene glycol, as shown in Figure 2.6. (Hu & Yang 2000)
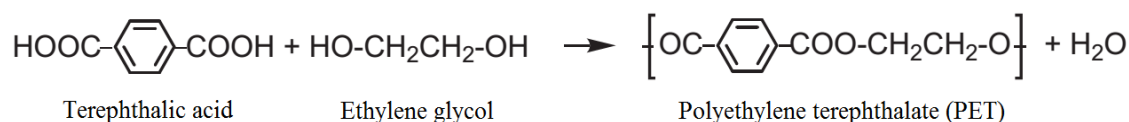
Figure 2.6. Polycondensation reaction between terephthalic acid and ethylene glycol, adapted from (Hu & Yang 2000).

PET is a semicrystalline, thermoplastic polymer, which has excellent fiber forming properties due to its high crystallinity and melting point. The melting point and glass

transition temperature of PET are 265 °C and 65−105 °C, respectively. PET fiber has many outstanding properties, for example high elastic modulus and breaking tenacity, good heat setting properties, and good thermal and light resistance. PET fiber is also highly resistant to oxidation and reduction, it can withstand severe bleaching, it has good resistance against most of the common organic solvents and hydrocarbon oils, and it has low moisture regain. (Ebnesajjad 2013, pp. 94–95; Michler & Baltá-Calleja 2012, p. 270; Hu & Yang 2000)

PET is used in a wide range of applications, including synthetic fibers, food and beverage containers, V-belts and conveyor belts. In the medical field, PET is used as sutures, wound dressings, and scaffolds, and it is an especially popular material used in prosthetic vascular grafts. For vascular applications, PET is usually manufactured in woven or knitted form. (Ebnesajjad 2013, pp. 94–95; Alagirusamy & Das 2010, p. 470; McKeen 2010, p. 100; Hu & Yang 2000)

2.3.2 Melt Spinning

Fiber-based polymer scaffolds used in cell culturing are manufactured via methods that are familiar from the textile industry. Polymer fibers can be manufactured by a number of methods, one of which is called melt spinning. Melt spinning is probably the simplest way to produce fibers, since neither solvent addition nor removal is necessary. Thus, melt spinning is often used for polymers which are able to melt without thermal degradation. Also, the polymer has to be thermally stable over a range of temperatures so that the correct extrusion viscosity can be achieved. (Mather & Wardman 2011, p. 130; van Blitterswijk 2008, p. 426)

PET fibers are typically produced via melt spinning process, where the polymer melt is forced through a mold called a spinneret. A spinneret contains tiny capillary holes and the diameter of a hole is usually 100−400 μm. The number of the spinneret holes vary depending on the application. (Hu & Yang 2000) In addition to a spinneret, a melt spinning machinery typically consists of an extruder, a metering pump and a filter pack (Mather & Wardman 2011, p. 130). Figure 2.7 shows a schematic illustration of the melt spinning process.
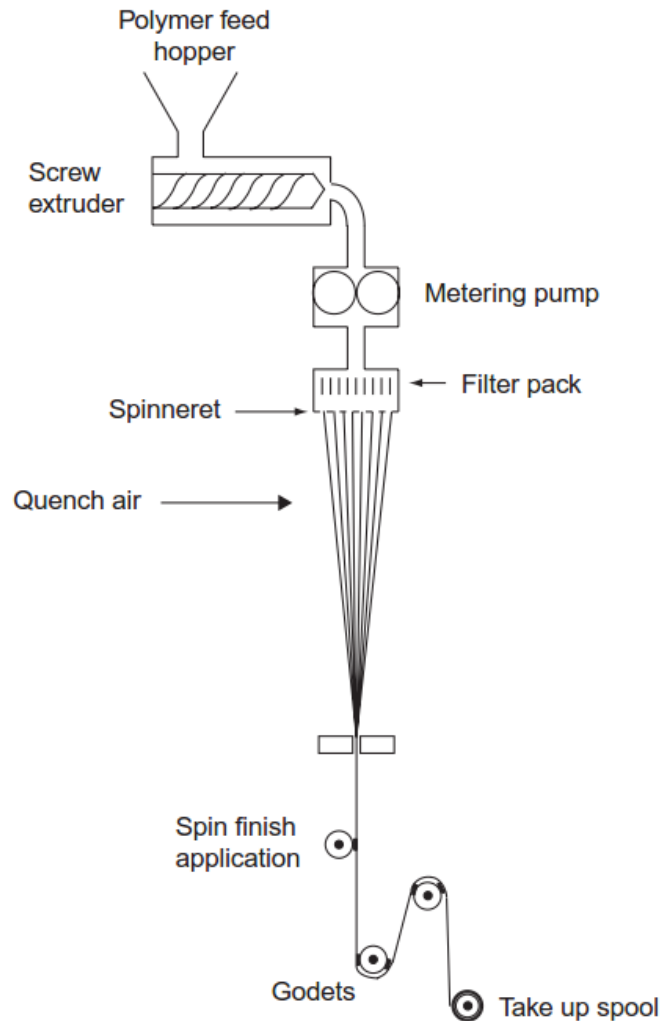
Figure 2.7. *Typical melt spinning process (Mather & Wardman 2011, p. 131). First, the polymer granules are fed in the screw extruder via polymer feed hopper. The granules are melted and the extruder screw brings the molten and compressed polymer towards the metering pump. The metering pump ensures that the polymer melt flows continuously through the filter pack, which in turn prevents the solid impurities from getting in the spinneret. Spinneret contains tiny capillary holes, through which the polymer melt passes. The formed filaments are cooled in quench air and gathered into a multifilament yarn, which might be treated with a spin finish application. Finally, the yarn reaches the roller.*

In the melt spinning process, polymer granules are fed in the screw extruder via polymer feed hopper. The screw extruder contains heated chambers. The polymer granules are melted and the screw brings the molten and compressed polymer towards the metering pump, which ensures the continuous flow of the polymer melt through the filter pack and finally through the spinneret's holes. The filter pack prevents the solid impurities from getting in the spinneret. After the polymer melt has passed through the spinneret, the fiber filaments are cooled in quench air and gathered into a multifilament yarn. The yarn might be treated with a spin finish application. Finally, the yarn reaches the roller. (Mather & Wardman 2011, p. 130)

The velocity at which the filaments come out from the spinneret is typically much lower than the take-up velocity at the roller. Therefore the filaments stretch, which improves the mechanical properties of the filaments due to the ordering of the polymer chain structure. To further improve the quality of the yarn, melt spinning process is usually followed by drawing (stretching). During drawing, the filaments are stretched, for example by factors of five to ten times or even more. (Mather & Wardman 2011, pp. 130–131)

2.3.3 Weaving

Weaving is a conventional and basic textile technique which can also be used to fabricate tissue engineering scaffolds. Weaving enables the formation of textile structures with controllable properties, such as porosity, morphology, and strength. (Tamayol et al. 2013) Some microstructural and mechanical properties of textile scaffolds made by weaving were already given in Table 2.2.

Two distinct sets of yarns are needed in the process of fabricating woven textiles. One of the sets is a cross-wise set ('weft') and the other is a length-wise set ('warp'). The fabric is formed by interlacing the weft and the warp at 90° to each other. Weaving process is conducted by a machine called a 'loom' (Figure 2.8). (Akovali et al. 2012, p. 157)
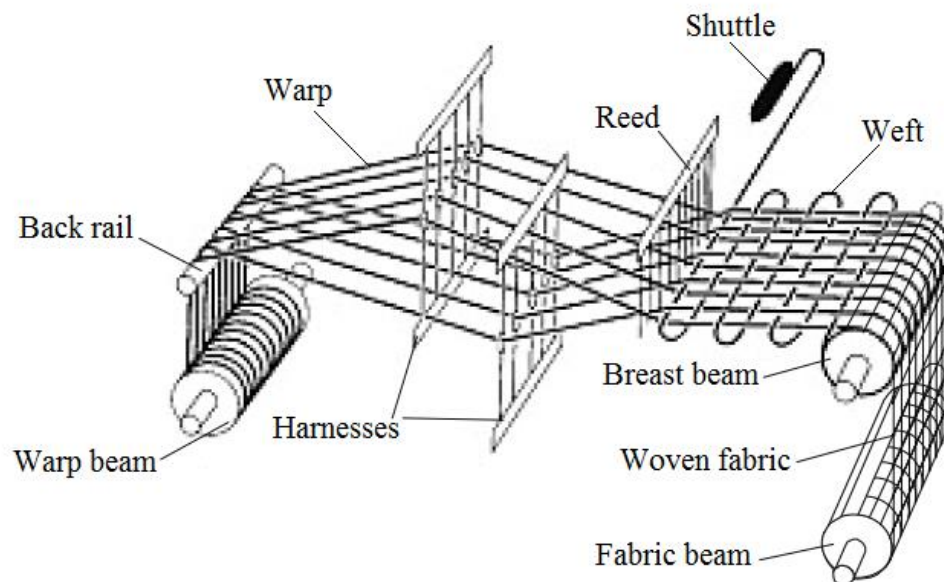
Figure 2.8. *A weaving loom and its main parts, adapted from (Wulfhorst et al. 2006, p. 134).*

The weaving system contains a series of frames that are called 'harnesses'. Warp yarns are threaded into a loom through harnesses, which, during the weaving process, raise certain warp yarns above the others. This creates a space ('shed') between the raised and non-raised warp yarns, and the weft is carried through the shed by a 'shuttle', where the

weft is placed in. The harnesses are moved for each pass of the shuttle and a reed pushes the weft to its intended position. The movement of the harnesses determines the type of the weave pattern. (Akovali et al. 2012, p. 157) Figure 2.9 shows a few typical weave patterns.
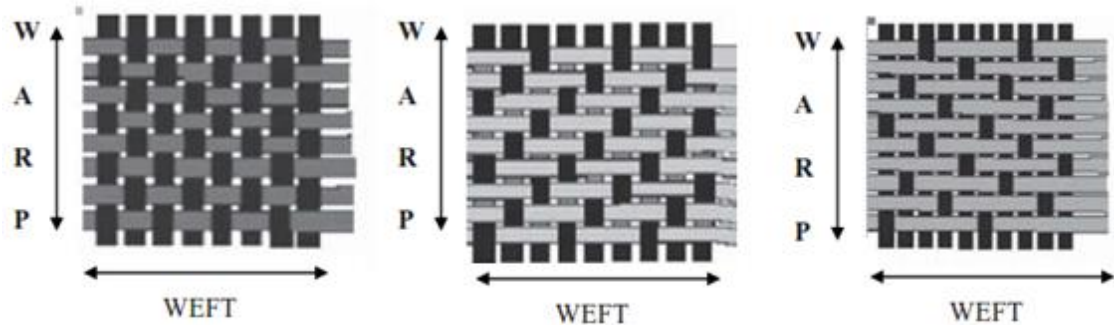
Figure 2.9. Typical weave patterns. From left to right: plain weave, twill weave and satin weave. Adapted from (Akovali et al. 2012, p. 163).

Plain weave is formed by passing yarns alternatively over and under each other. Thus, there are maximum number of interlacing points. It is the simplest and least expensive weave to produce. Plain weave is similar in both sides of the textile. In a *twill weave*, the interlacing points of the weft and warp yarns are located so that they form a diagonal pattern. The interlacing points float by one to the right or left. In a *satin weave*, the interlacing points float by greater than one to the right or left, and it has the least interlacing points. (Akovali et al. 2012, pp. 161–163)

2.4 Previous Studies

The immaturity of hPSC-CMs is an issue which is delaying progress in the field of cardiac tissue engineering. hPSC-CMs are found to be able to undergo structural and functional maturation when transplanted into the working myocardium of model species (van Laake et al. 2007). The observation shows, that these cells are able to mature when placed in a suitable environment, and there have been many attempts to find suitable stimuli for the *in vitro* maturation of the cells. (Denning et al. 2015) Some strategies are visualized in Figure 2.10.
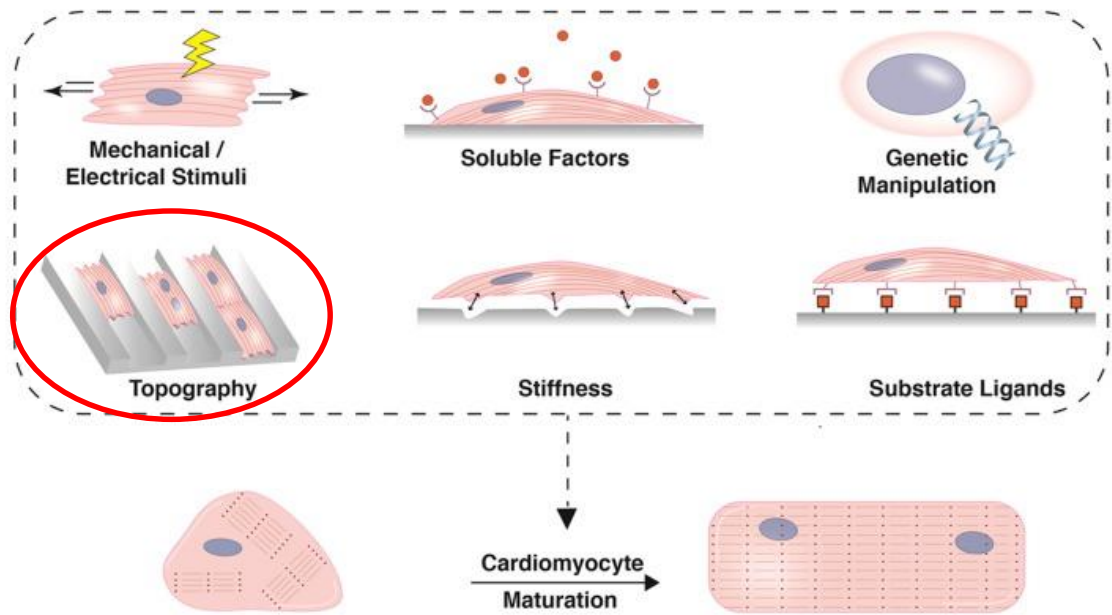
Figure 2.10. In vitro *maturation strategies for hPSC-CMs, adapted from (Denning et al. 2015). The strategies include biophysical, biochemical, genetic and environmental inducers. Here, the concentration will be on topography (circled in red).*

As Figure 2.10 shows, the *in vitro* maturation strategies include biophysical, biochemical, genetic and environmental inducers to improve the maturation of hPSC-CMs. Here, the concentration will be on cell culture substrates' topography. The amount of published studies aiming for improving the maturation of hiPSC-CMs using the topography strategy is quite limited. Rather than hiPSC-CMs, most of the studies investigating CMs' maturation are utilizing either hESC-CMs (for example, Salick et al. (2014) and Zhang et al. (2013)) or murine CMs (for example, Wang et al. (2011) and McCain et al. (2014)). Next, previous studies using both hiPSC-CMs and topography strategy are described briefly.

One of the strategies for studying the effect of substrate topography on hiPSC-CMs' maturation is using fiber structures as culture substrates. A study used copolymer fiber matrices. Ring opening polymerization of monomeric ε-caprolactone with methoxy polyethylene glycol at selected molar ratios was used for the generation of the copolymers. The most suitable combination was found to be polyethylene glycol (PEG) + polycaprolactone (PCL), the molar ratios being 4 % and 96 %, respectively. PEG is a biocompatible and hydrophilic polymer, whereas PCL is a biodegradable and hydrophobic polymer. The polymers were electrospun on glass coverslips to form fiber mesh scaffolds mimicking ECM's structure. The fibers had the average diameter of 0.6 μm. The study showed that, compared to other test substrates, the cells grown on 4%PEG-96%PCL scaffolds exhibited more organized sarcomeres, increased contractility and higher expression of genes associated with cardiac maturation. (Chun et al. 2015)

In another study hiPSC-CMs were cultured on a highly aligned nanofiber cardiac patch. Two scanning electron microscope (SEM) images of hiPSC-CMs growing on the nanofibers are presented in Figure 2.11. The nanofibers were made of polylactide-co-glycolide (PLGA) by electrospinning, and the average fiber diameter was 0.95 μm. The nanofibers were deposited onto a custom manufactured rotating wheel, and the scaffolds were approximately 50 μm thick. The cells grown on aligned nanofibers were compared to cells grown on flat surfaces. Both of these cell culture substrates were coated with 1 % gelatin before seeding the cells. The cells grown on nanofibers exhibited more adult-like shape by stretching and elongating along the orientation of the aligned fibers. Also, the cells grown on nanofibers had longer sarcomeres (≈1.68 μm) than the control cells cultured on flat culture plates (≈1.59 μm). Also, in contrast to the control cells, the cells grown on nanofibers assembled into well-organized myofibrils with clear aligned Z-discs, and they exhibited enhanced calcium cycling. (Khan et al. 2015)
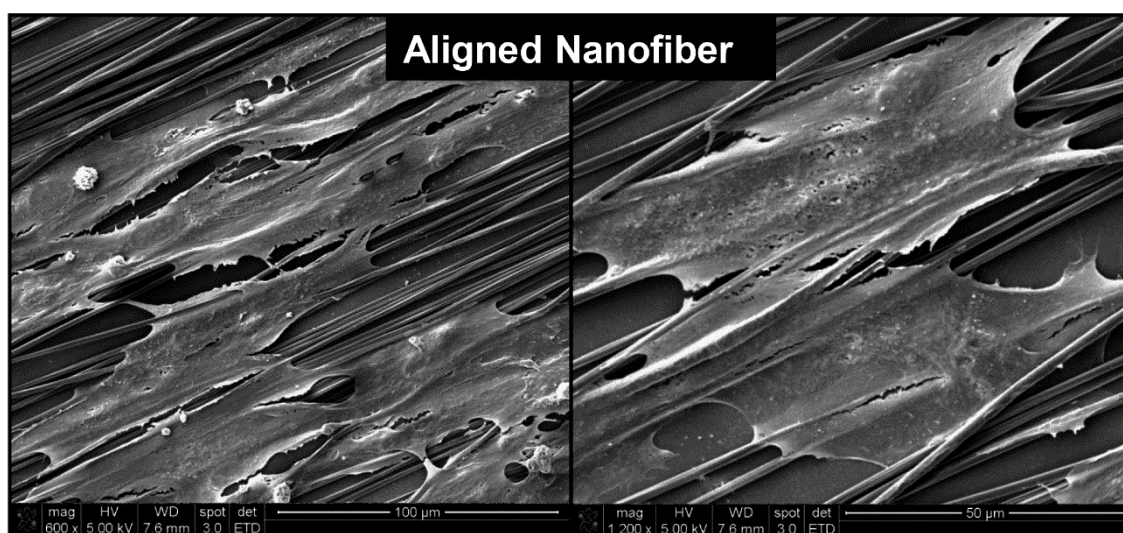
Figure 2.11. SEM images of hiPSC-CMs growing on aligned nanofibers, adapted from (Khan et al. 2015). The length of the scale bar is 100 μm on the left image and 50 μm on the right image.

A study carried out by Han et al. (2016) investigated if the maturation of hiPSC-CMs could be improved by culturing the cells on aligned electrospun fibrous scaffolds made of PCL. In addition to aligned fibrous scaffolds, the cells were cultured on random fibrous scaffolds, and also on flat culture substrates as a control. All of these substrates were coated with Matrigel. SEM images of the aligned and random fibrous scaffolds are presented in Figure 2.12. The fibrous scaffolds were approximately 100 μm in thickness and the average fiber diameter was approximately 0.7 μm. The hiPSC-CMs cultured on aligned fibrous scaffolds became elongated and extended in the direction parallel to the fiber alignment, but the hiPSC-CMs cultured on random fibrous scaffolds remained circular and stayed together. The hiPSC-CMs grown on flat culture substrates formed randomly oriented large cellular bundles. These results showed that hiPSC-CMs anisotropic alignment was induced by aligned fibrous scaffolds. It was also found out,

that the cells grown on aligned fibrous scaffolds exhibited improved sarcomere organization and increased expression of cardiac genes. However, the calcium handling properties of the hiPSC-CMs grown on aligned fibrous scaffolds were not improved. The study suggested that using cell alignment inducing scaffolds, as a single method, has limited effect on enhancing the hiPSC-CMs' maturation.
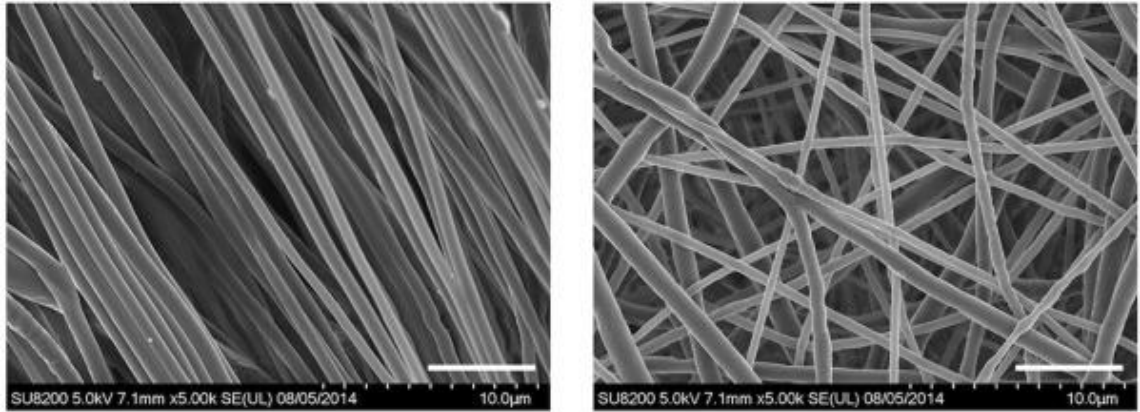
Figure 2.12. SEM images of aligned (left) and random (right) fibrous scaffolds, adapted from (Han et al. 2016). The lengths of the scale bars are 10 μm in both images.

Another strategy for studying the effect of substrate topography on hiPSC-CMs' maturation is micropatterning. A study investigated the effect of microgrooved substrates on calcium cycling of hiPSC-CMs. The hiPSC-CMs grown on microgrooved substrates were compared to hiPSC-CMs grown on flat surfaces (Figure 2.13). (Rao et al. 2013)
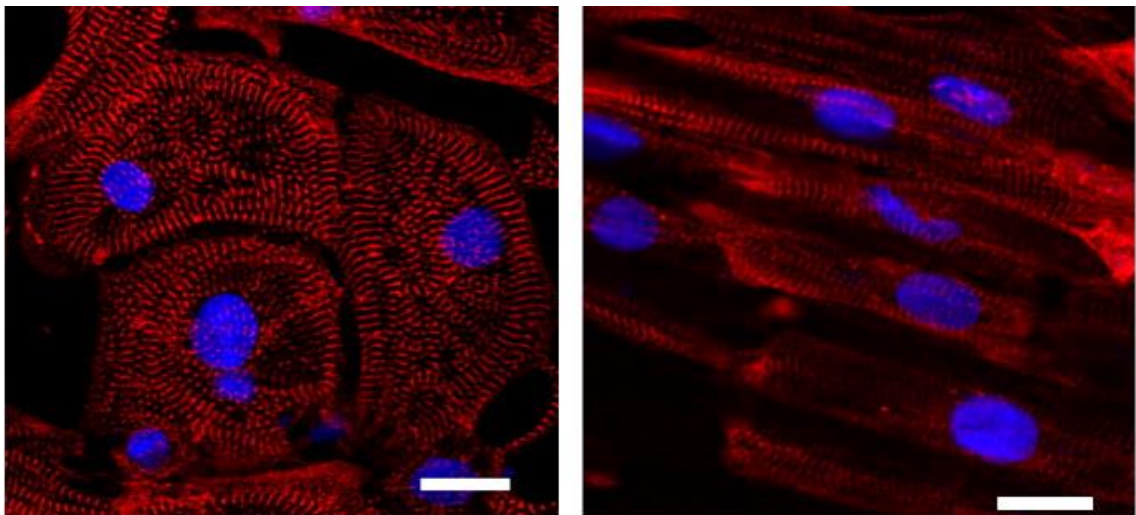
Figure 2.13. Immunofluorescence images of hiPSC-CMs grown on flat substrate (left) and microgrooved substrate, adapted from (Rao et al. 2013). The myofibrils are seen in red (α-actinin). The nuclei are seen in blue (DAPI). In the left image, the cells are irregularly shaped and have disorganized sarcomeres, whereas in the right image the cells are more rod-like in shape and the sarcomeres are more organized. The lengths of the scale bars are 20 μm in both images.

The cells were seeded onto fibronectin coated microgrooved culture substrates made of polydimethylsiloxane (PDMS), which is a biologically inert, non-toxic polymer. The grooves were 10 μm in width, 4 μm in depth, and the grooves were 10 μm apart. These dimensions were chosen due to a preliminary study made with neonatal rat ventricular myocytes (NRVM), which presented that grooves of this width modified the calcium cycling properties of CMs most effectively. (Rao et al. 2013) Also, according to Robertson et al. (2013), the width of an adult CM is approximately 10 μm. The control cells were cultured on unstructured PDMS membranes. The study concluded, that microgrooved culture substrates induced cellular alignment and more organized sarcomere structures in addition to improved calcium cycling (Rao et al. 2013).

Another study utilizing micropatterning for improving the functional maturation of hiPSC-CMs was carried out by Ribeiro et al. (2015). The hiPSC-CMs were seeded on polyacrylamide gel patterned with 1 % gelatin lines. The gelatin lines were 20 μm in width and they were 20 μm apart. The hiPSC-CMs were seeded on these lines, and they were compared to human fetal CMs cultured on same kinds of substrates. The study showed that by adjusting the culture conditions the contraction stress of a single hiPSC-CM could be increased to values higher than those of human fetal CMs. Also, the hiPSC-CMs exhibited electrophysiological maturation, increased expression of cardiac genes, and improved sarcomere organization.

3. AIMS OF THE STUDY

The aim of this study was to find out whether the structural maturation of hiPSC-CMs can be enhanced by growing them on woven PET textile structures. A visual comparison of hPSC-CMs and adult human CMs is shown in Figure 3.1.
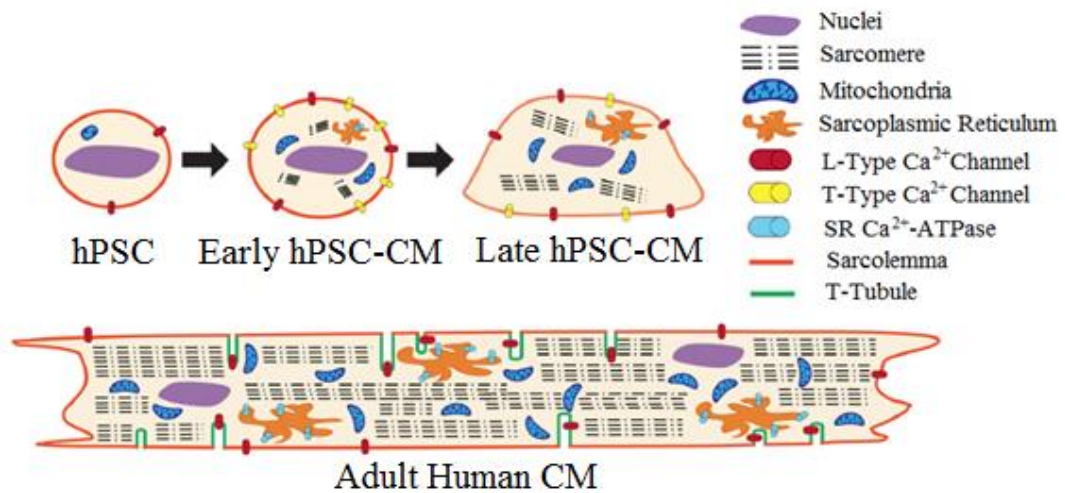
Figure 3.1. *A visual morphology comparison between hPSC-CM and adult CM, adapted from (Robertson et al. 2013).*

When grown on a flat surface, for example on a Petri dish, hiPSC-CMs tend to become circular and irregularly shaped, whereas adult CMs are rod-like. Also, the sarcomere structures in hiPSC-CMs are disarrayed, unlike in adult CMs, where the sarcomeres are highly organized. In addition, adult CMs may have multiple nuclei, while hiPSC-CMs are mononucleated.
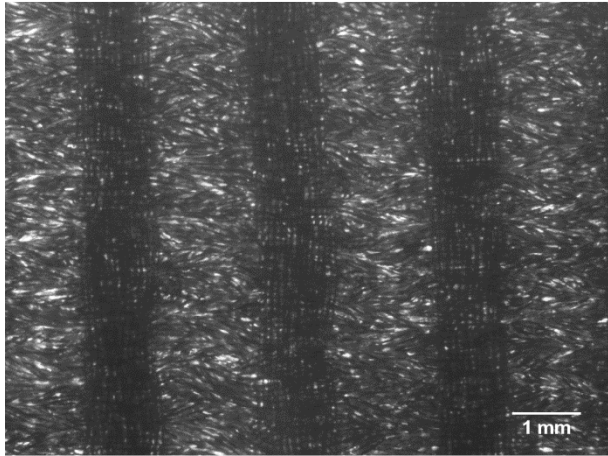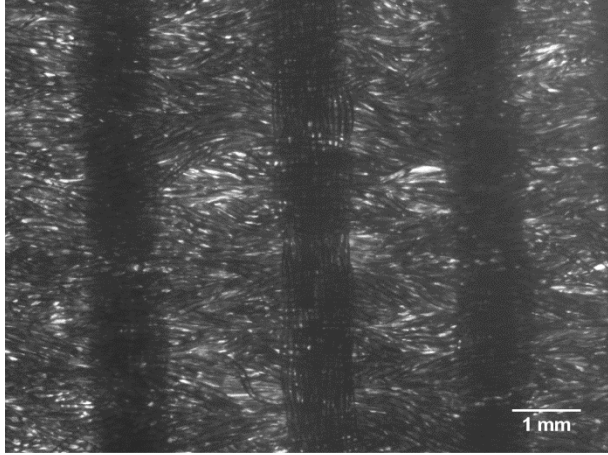
The hypothesis is that hiPSC-CMs will become morphologically more mature when grown on textile structure. The textile topography is expected to guide the cell growth so that the hiPSC-CMs would become more rod-like in shape. Also, the growing along the fibers is expected to have a positive effect on the sarcomere structure organization.

4. MATERIALS AND METHODS

4.1 Materials
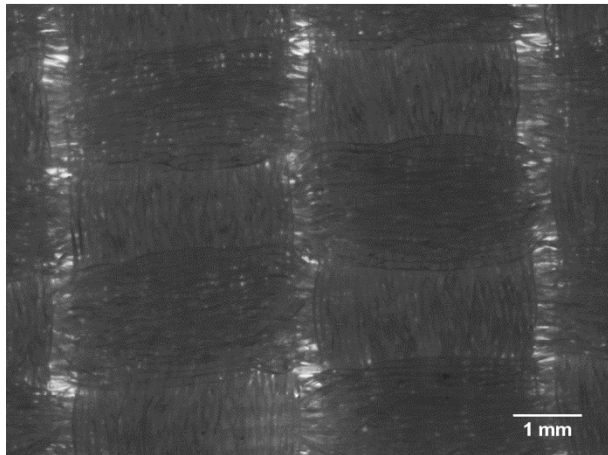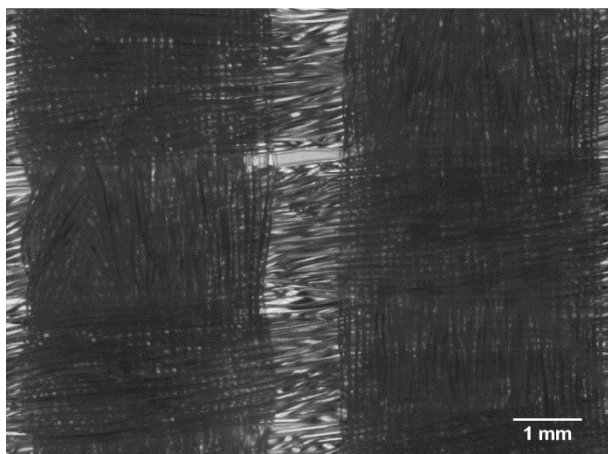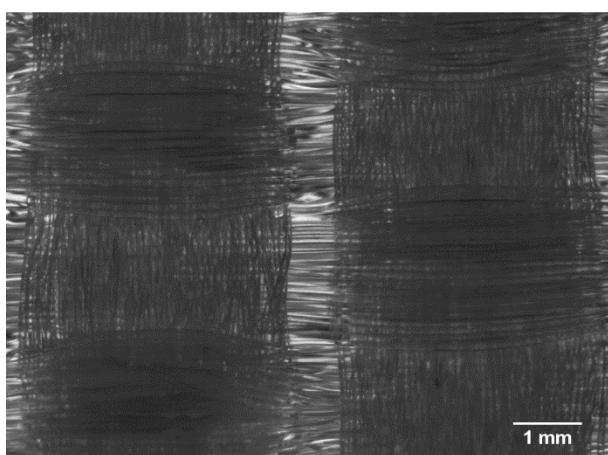
In this study, hiPSC-CMs were grown on five different PET textile structures. Textiles were labelled by consecutive numbering: PET1, PET2, PET3, PET4 and PET5. PET4 and PET5 were produced in Tampere University of Technology, and they were blue in color (Table 4.1). The yarn used for weaving the textiles was a PET multifilament yarn (Finn-Nauha Oy, Haapamäki, Finland). The yarn was 78 dtex (g/10,000 m) in fineness and 20 turns/meter in twist. Each yarn consisted of 24 filaments. The structure of PET4 was a plain weave, and the structure of PET5 was a plain weave derivate. (Stenlund 2013)

Table 4.1. Textiles produced in Tampere University of Technology. The images were taken with a Zeiss Axio Vert.A1 microscope and AxioCam MRc5 camera; 5x objective was used. In the figures, the warp yarns are horizontal and the weft yarns are vertical.

Name and details	Structure	Manufacturer
PET4; blue, heat treated		*Yarn*: Finn-Nauha Oy, Haapamäki, Finland *Textile*: Tampere University of Technology
PET5; blue, heat treated		*Yarn*: Finn-Nauha Oy, Haapamäki, Finland *Textile*: Tampere University of Technology

By contrast, PET1, PET2 and PET3 were commercial, colorless (transparent) textiles produced by Inka Oy (Killinkoski, Finland). The textile structures are presented in Table 4.2.

Table 4.2. Commercial textiles used in this study. The images were taken with a Zeiss Axio Vert.A1 microscope and AxioCam MRc5 camera; 5x objective was used. In the figures, the warp yarns are horizontal and the weft yarns are vertical.

Name and details	Structure	Manufacturer
PET1; colorless, heat treated, textured yarn		Inka Oy, Killinkoski, Finland
PET2; colorless, heat treated, textured weft yarn		Inka Oy, Killinkoski, Finland
PET3; colorless, heat treated, textured yarn		Inka Oy, Killinkoski, Finland

There was not much information provided about the commercial textiles. In PET2, the weft yarn was a textured yarn. In PET1 and PET3, both warp and weft yarns were textured. All the textile samples (PET1–PET5) were heat treated in Tampere University of Technology in order to flatten the textiles so that the imaging of the samples would be easier.

The fiber (filament) diameters were measured from immunostained images by using ImageJ software and utilizing the autofluorescence of the textiles, which was seen with Alexa Fluor 568 (red) and 488 (green). Autofluorescence makes the fibers visible, even though only the stained cell structures should be seen. This enabled the measurement of fiber diameters by using ImageJ's line selection tool: a straight line was drawn from fiber's edge to the other edge perpendicular to the longitudinal axis of the fiber, and the length of the drawn line was measured with the software. The measurements were done for multiple images of each textile and the average value was calculated. For each textile, 10 measurements were used for calculating the average fiber diameter. The diameters were 20−25 μm for all the textiles, and the averages ± standard deviations are presented in Table 4.3.

Table 4.3. *Average fiber diameters ± standard deviations.*

Sample	Average fiber diameter (μm)
PET1	24.4 ± 1.82
PET2	23.2 ± 1.43
PET3	22.9 ± 1.91
PET4	20.4 ± 1.53
PET5	22.0 ± 1.42

Control samples were generated by plating hiPSC-CMs on glass coverslips (13 mm in diameter) instead of PET textiles. The cell line used in this study was a control cell line UTA04602.WT produced from a healthy individual. The textiles and coverslips were coated with 0.1 % gelatin passively at room temperature for one hour. A table of used reagents and their suppliers and/or manufacturers which will not be mentioned in Chapter 4 is provided in Appendix D.

4.2 Workflow

The workflow of the study is illustrated in Figure 4.1. The first step was to differentiate hiPSCs to CMs (Subchapter 4.3), which took two weeks. In the next step, dissociation, beating CM aggregates were collected and single cells were plated on PET textiles (Subchapter 4.4). After the culturing period, the analyzing of samples started on day 27. On day 27, samples were analyzed with live/dead imaging (Subchapter 4.5), and the immunostaining protocol (Subchapter 4.6; Appendix B) was started by fixing the cells.

The immunostaining protocol was continued on day 28 and finished on day 29, after which the samples were imaged with a fluorescence microscope.

Day 1: Cardiomyocyte differentiation	Day 6: Medium change (0% KO-SR hES)	Day 8: Medium change (0% KO-SR hES)
Day 13: Medium change (0% KO-SR hES)	Day 15: Medium change (10% KO-SR hES)	Day 17: Dissociation, plating of hiPSC-CMs on PET
Day 20: Medium change (EB medium)	Day 24: Medium change (EB medium)	Day 27: Live/dead imaging, fixing of hiPSC-CMs
Day 28: Double fluorescence protocol started	Day 29: Double fluorescence protocol finished	Day 30: Imaging of immunostained hiPSC-CMs

Figure 4.1. The workflow of the study.

In total, the workflow was carried out five times. The steps of the workflow are explained in the following subchapters in further detail. The sarcomere orientation and length were analyzed from the immunostained images with a software called CytoSpectre (Subchapter 4.7), which allows the automatic quantification of these structural properties in microscopy images (Kartasalo et al. 2015). Also, the method for evaluating statistical significance is presented in Subchapter 4.8.

4.3 Cardiomyocyte Differentiation

The cell line used in this study (UTA04602.WT) was generated from dermal fibroblasts of a healthy 55-year-old female by Heart Group of BioMediTech, Tampere. In this study, the laboratory work started from the cardiomyocyte differentiation. The differentiation of hiPSCs to cardiomyocytes was carried out by using mouse endodermal-like (END-2) cell

co-culture protocol. hiPSC colonies were plated on END-2 cells which give cardiomyocyte differentiation promoting substances to the medium (Mummery et al. 2003; Passier et al. 2005).

Mitomycin C treated END-2 cells were plated on 12-well plates a day before differentiation. The next day the plated END-2 cells were visually evaluated, after which the differentiation protocol could be started. The first step was to change 0 % KO-SR hES medium supplemented with 2.29 mg/ml ascorbic acid (Table 4.4) to the END-2 cells containing well plates about an hour before plating the iPSC colonies. The quantity of ascorbic acid added was 0.7 ml of 50 mg/ml stock solution to 12 ml of medium.

Table 4.4. Contents of 0 % KO-SR hES medium.

Volume	Ingredient	Quantity
48.75 ml	KO-DMEM	
0.5 ml	NEAA	1 %
0.5 ml	GlutaMax	2 mM
0.25 ml	Pen/Strep.	50 U/ml
97.5 µl	β-mercaptoethanol	0.1 mM
(2.8 ml	Ascorbic Acid (added just before use))	3.0 mM

The next step was to separate the mouse embryonic fibroblast (MEF) feeder layer from the 6-well plates containing the hiPSC colonies. This was done by pipetting. The procedure had to be gentle enough so that as small amount of iPSC colonies as possible was removed with MEF layer. When the MEF layer was detached from the well plate and the iPSC colonies, the pieces of MEF layer were swirled to the center and removed.

Next, the hiPSC colonies were scraped to the culture medium as whole as possible. The colonies were swirled to the center of the well, from where the colonies were aspirated with a pipette and plated on the END-2 cells. hiPSC colonies from one well were dealt into four END-2 wells. After plating the colonies, the well plates were manually shaken a bit in order to spread the colonies evenly across the wells. The plates were stored in 37 °C incubator. On days 6, 8, and 13 0 % KO-SR hES medium was changed to the cells. On day 15, the medium was changed to 10 % KO-SR hES medium (Table 4.5).

Table 4.5. Contents of 10 % KO-SR hES medium.

Volume	Ingredient	Quantity
43.75 ml	KO-DMEM	
5 ml	KO-SR	10 %
0.5 ml	NEAA	1 %
0.5 ml	Glutamax	2 mM
0.25 ml	Pen/Strep.	50 U/ml
97.5 µl	β-mercaptoethanol	0.1 mM

After day 15 the media were changed three times a week. The first beating aggregates usually appeared between days 8 and 14. Most of the beating aggregates appeared before day 21 but new beating areas could still appear until day 30. In this study, the dissociation of beating aggregates was carried out on day 17.

4.4 Dissociation of Beating Aggregates

On day 17, the beating aggregates were isolated from 12-well plates with a microscalpel and collected into culture medium. When enough areas were collected (one beating aggregate per sample for imaging, two beating aggregates for RNA extraction), the 10 % KO-SR hES medium was removed and the excised tissue was washed in Low-Ca (Table 1, Appendix A) for 30 minutes at room temperature. Then, buffer 1 was removed and replaced with Enzyme medium (Table 2, Appendix A), in which the areas were incubated for 45 minutes at 37 °C. During the time of incubation, both PET textiles and coverslips were disinfected with 70% ethanol and dried.

After the incubation, buffer 2 was removed and replaced with a KB medium (Table 3, Appendix A), in which the beating areas were washed for an hour at room temperature. The PET textiles and coverslips were coated with 0.1 % gelatin during that time. Then, buffer 3 was replaced with EB medium (Table 4.6), where the aggregates were broken down by pressing pipette's tip against the well plate's bottom and pipetting the solution up and down several times.

Table 4.6. Contents of EB medium (20% FBS KO-DMEM).

Volume	Ingredient	Quantity
38.75 ml	KO-DMEM	
10 ml	FBS	10 %
0.5 ml	NEAA	1 %
0.5 ml	Glutamax	2 mM
0.25 ml	Pen/Strep.	50 U/ml

After that, 50 μl of cell suspension was plated on every PET textile and coverslip. The samples were incubated for 45 minutes at 37 °C after which 650 μl of warm EB medium was pipetted into every well. Textile samples in EB medium on a 24-well plate are shown in Figure 4.2.
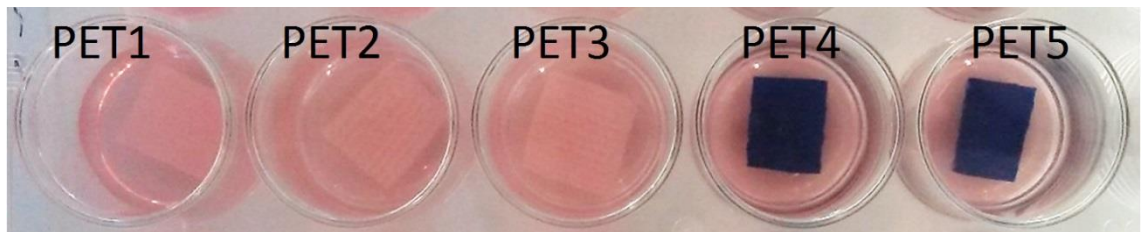
Figure 4.2. PET textile samples in EB medium on a 24-well plate.

The media were changed on days 20 and 24. The analyzing of samples started on day 27. Analyzing methods included live/dead imaging, immunocytochemistry and fluorescent microscopy.

4.5 Live/Dead Imaging

Live/dead imaging was done on day 27. hiPSC-CMs were stained with a live/dead staining kit (L3224 LIVE/DEAD® Viability/Cytotoxicity Kit for mammalian cells, Molecular Probes, Inc, Invitrogen). The kit included two fluorescent dyes: 1 mM Calcein AM (C-AM), which stains live cells in green (wavelength 488), and 2 mM Ethidium homodimer-1 (EtHD-1), which stains dead cells in red (wavelength 568). C-AM and EtHD-1 were thawed, spun down in centrifuge, and pipetted in warm EB medium (37 °C). The amounts of C-AM and EtHD-1 pipetted into 10 ml of EB medium were 2 μl and 5 μl, respectively.

500 µl of live/dead stain solution was prepared for each sample. The samples were incubated for 30 minutes in 37 °C before starting the imaging. Live/dead imaging was performed using an Olympus BX61WI water immersion fluorescence microscope and

Hamamatsu ORCA-ER (Model C4742-80-12AG) camera. The samples were imaged in EB medium on a Petri dish using 10x and 40x objectives.

4.6 Immunocytochemistry and Fluorescent Microscopy

The hiPSC-CMs were stained using a double-fluorescence protocol (Appendix B). The protocol was started by fixing the cells on day 27, continued on day 28 and finished on day 29. Primary antibodies used were goat cardiac troponin T (ab64623, Abcam) and mouse myosin-binding protein C (MYBPC) (sc-166081, Santa Cruz). Secondary antibodies used were Alexa Fluor 568 donkey anti-goat (Life Technologies) and Alexa Fluor 488 donkey anti-mouse (Life Technologies). The localization of stained sarcomere proteins, myosin-binding protein C and troponin T, are shown in Figure 4.3.
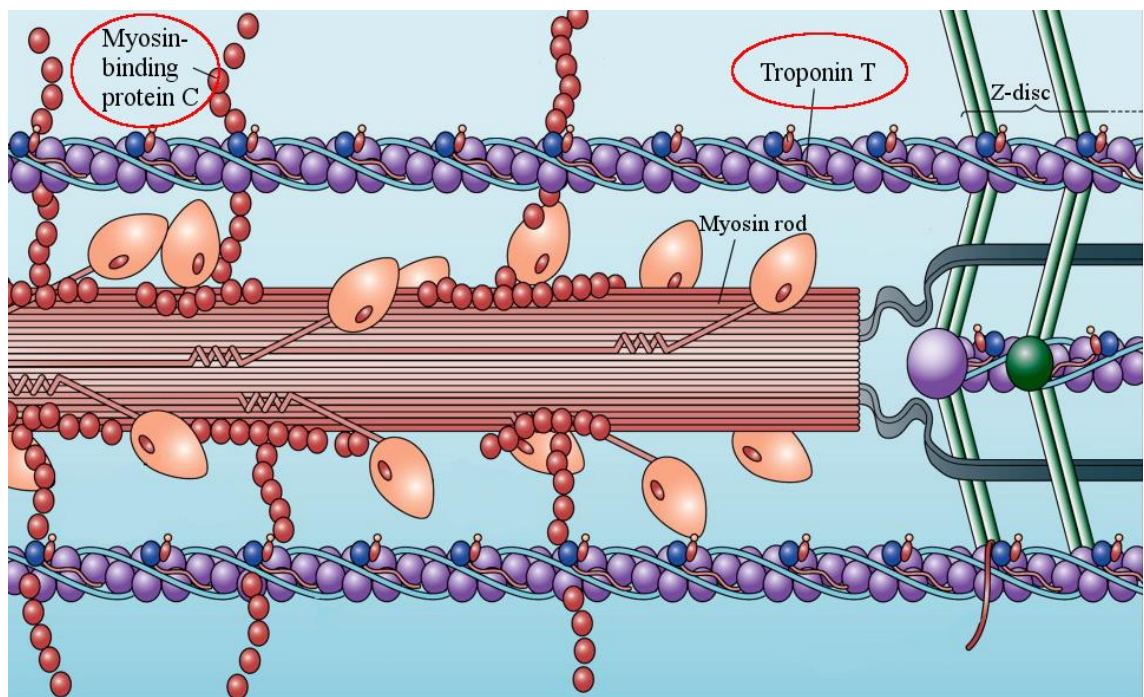
Figure 4.3. *Localization of studied cardiomyocyte sarcomere proteins, adapted from (Maron & Maron 2013).*

After the double-fluorescence protocol was carried out, the samples were mounted on microscope slides (Menzel-Gläser, Thermo Scientific) with a Vectashield Mounting Media with DAPI (H-1200, Vector Lab), which stains the nuclei of the cells. The samples were imaged on day 30 with a Zeiss Imager.M2 Axio fluorescence microscope with ApoTome and AxioCam MRm camera. Z-stack images were taken with a 40x oil immersion objective. The images were processed with ImageJ software.

4.7 Analysis of Sarcomere Orientation and Length

The sarcomere orientation and length were analyzed from the immunostained images with a software called CytoSpectre, which allows the automatic quantification of these

structural properties in microscopy images (Kartasalo et al. 2015). Before using the software, the images were rotated so that the fibers of the textiles were oriented in the same direction lengthwise. All the fibers, which had hiPSC-CMs growing on top of them, were set vertically, as illustrated in Figure 4.4. The direction parallel to the longitudinal axis was set to be 90°. By rotating the images, the sarcomere orientations of different cells relative to the longitudinal axis of the fibers could be compared with each other. The rotating of the images of hiPSC-CMs grown on coverslips was not necessary, since the cell culture substrate was flat and had no longitudinal direction.
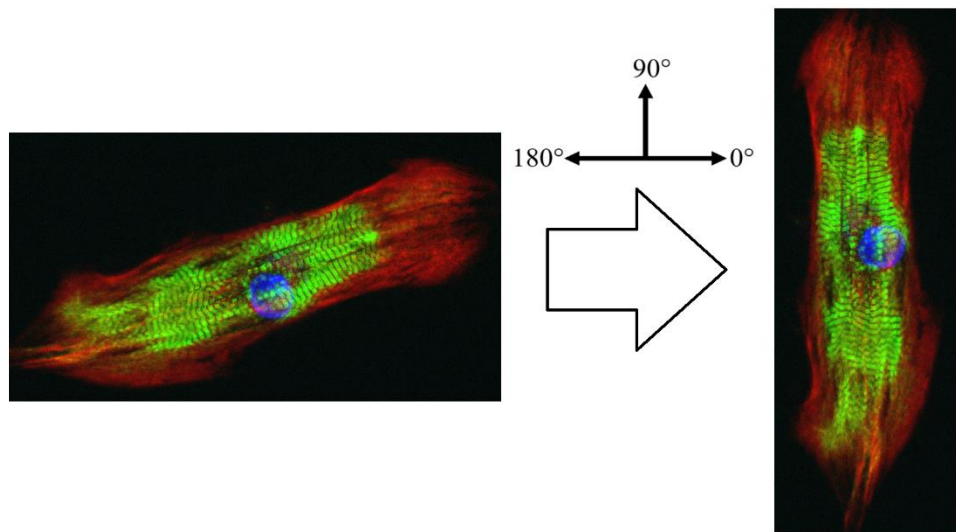
Figure 4.4. The images were rotated so that the sarcomere orientations of hiPSC-CMs grown on PET textiles could be analyzed as one group, and then be compared to the hiPSC-CMs grown on coverslips. The direction parallel to the longitudinal axis was set to be 90°.

Only the images of hiPSC-CMs with clearly showing sarcomeres were included in the analysis. If the signal-to-noise ratio was lower than one, the image was excluded from the analysis. The following properties were analyzed with the software: mean sarcomere orientation, mean sarcomere length, sarcomere length standard deviation, circular variance, and angular standard deviation.

Circular variance and angular standard deviation are measures for the spread of the orientation distribution. Circular variance can get values from 0 to 1. If all the sarcomeres were aligned along a single orientation, the circular variance would have a value close to zero. By contrast, if the sarcomere orientations were evenly distributed around the half circle (0°–180°), the circular variance would have a value close to one. Angular standard deviation can get values from 0 to $\sqrt{2} \approx 1{,}41$. Similarly to circular variance, angular standard deviation is low when the sarcomeres are aligned along a single orientation, and high when the orientations are evenly spread out around the half circle. (Kartasalo et al. 2015)

4.8   Statistical Analysis

Differences between hiPSC-CMs grown on PET textiles and coverslips were assessed by Student's t-test. The test used was an independent two-sample test assuming unequal variances. The p-values were calculated using Microsoft Excel and the values from two-tailed tests were used. The threshold for significant difference was $p < 0.05$.

The statistical significance was calculated for circular variance and angular standard deviation (measures for the spread of the sarcomere orientation distribution). Also, it was calculated for mean sarcomere length and sarcomere length standard deviation.

5. RESULTS

5.1 Imaging and Cell Shape

The structural maturation of hiPSC-CMs grown on PET textiles was evaluated by observing their structural properties and comparing them to those of hiPSC-CMs cultured on coverslips. The compared structural properties were morphology of the cells, sarcomere organization and orientation, and the length of sarcomeres. Also, the multinucleation of the cells was studied.

The cells were imaged with different kinds of microscopes. The morphology of cells grown on coverslips was observable with brightfield microscopy, whereas the cells grown on PET textiles were very difficult to detect without staining them and using a fluorescence microscope. Figure 5.1 illustrates the problem.
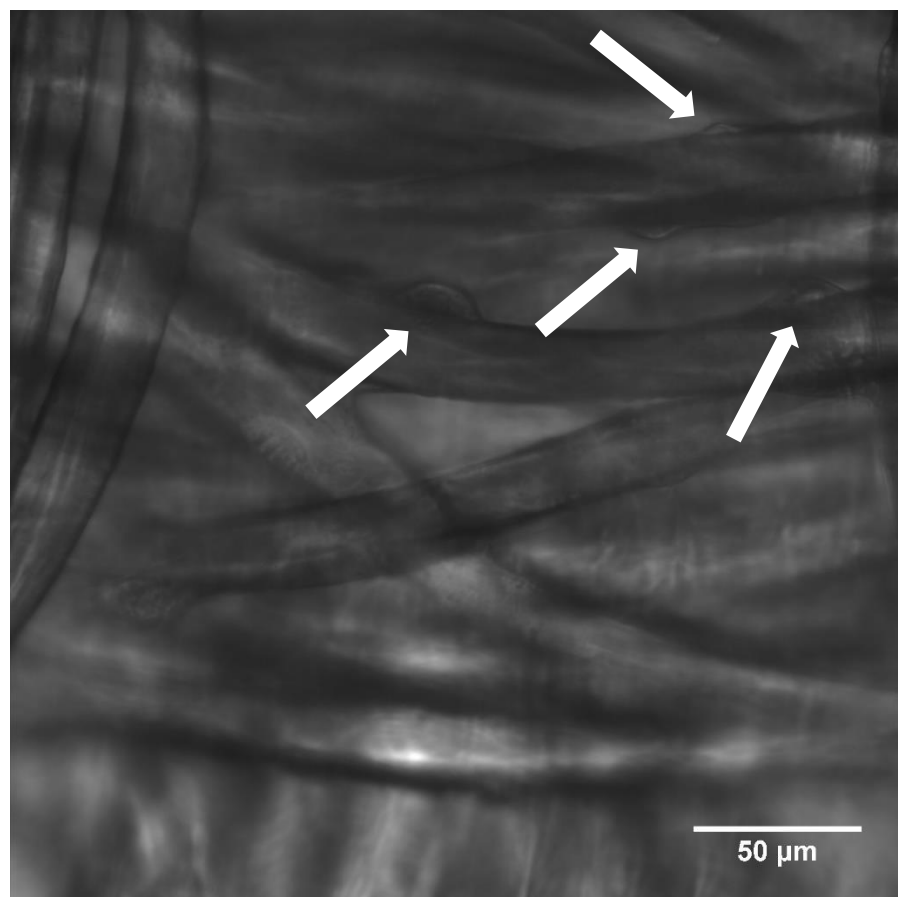
Figure 5.1. hiPSC-CMs were difficult to detect from the textiles without staining the cells. The arrows point to "bumps", which lie on the fibers and might be nuclei. The image was taken with Nikon TiE FN1 microscope and Hamamatsu ORCA-Flash 4.0 V2 camera.

The "bump", to which the arrow points in Figure 5.1, could be a nucleus, but it also might just be a lump of gelatin coating, impurity, etc. The cell structure is not visible in the image. In order to make the cells recognizable, the hiPSC-CMs grown on PET textiles had to be stained. Both live/dead staining and immunocytochemistry were used. Figure 5.2 shows a similar bump as seen in Figure 5.1, but the cell is immunostained with the double-fluorescence protocol.
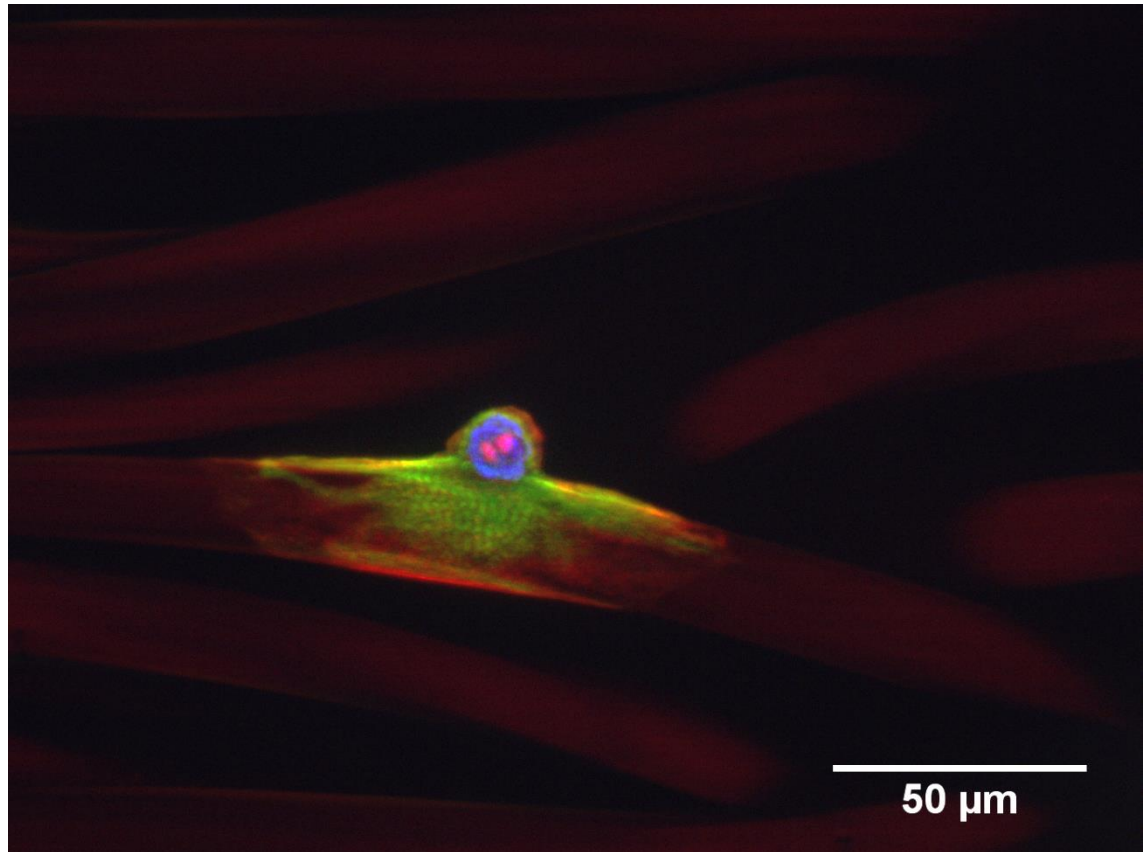
Figure 5.2. hiPSC-CM on PET4 textile. In the image, nucleus is seen in blue (DAPI), MYBPC is seen in green, and troponin T is seen in red. Also, there is some degree of autofluorescence, which makes the fiber structure show as well.

In Figure 5.2, the bump is clearly a nucleus, since it has been stained with DAPI (blue). In the image, the autofluorescence of PET textile makes it possible to see the fiber structure of the textile as well. PET4 and PET5, which were blue in color, showed the most autofluorescence, but autofluorescence occurred also with colorless textiles (PET1, PET2 and PET3).

Autofluorescence made the live/dead imaging challenging, and the method was found to be rather poor for imaging hiPSC-CMs grown on textiles, as can be seen in Figure 5.4 and Figure 5.5. Some of the most representable images taken of live cells are presented in Figure 5.3. The live/dead colors stained the whole cell.
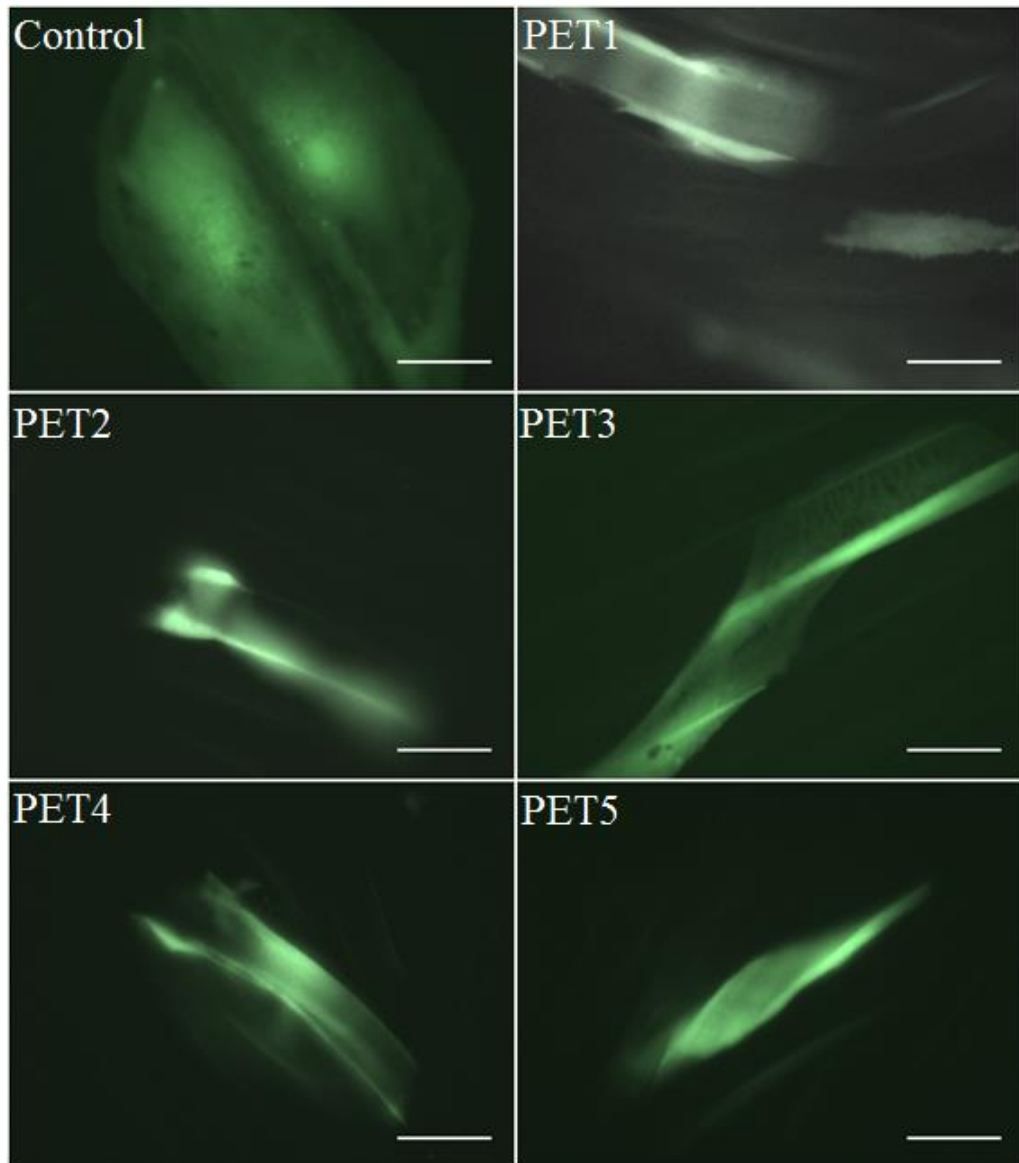
Figure 5.3. *Images of live cells, cells stained with live/dead stainings. The length of the scale bar is 20 μm.*

In Figure 5.3, the cells can be recognized quite well. However, sometimes it seemed like the cells had migrated between the fibers and inside the textile structure. In these cases, the fluorescent dye was "glowing" from under the fibers, as seen in Figure 5.4.
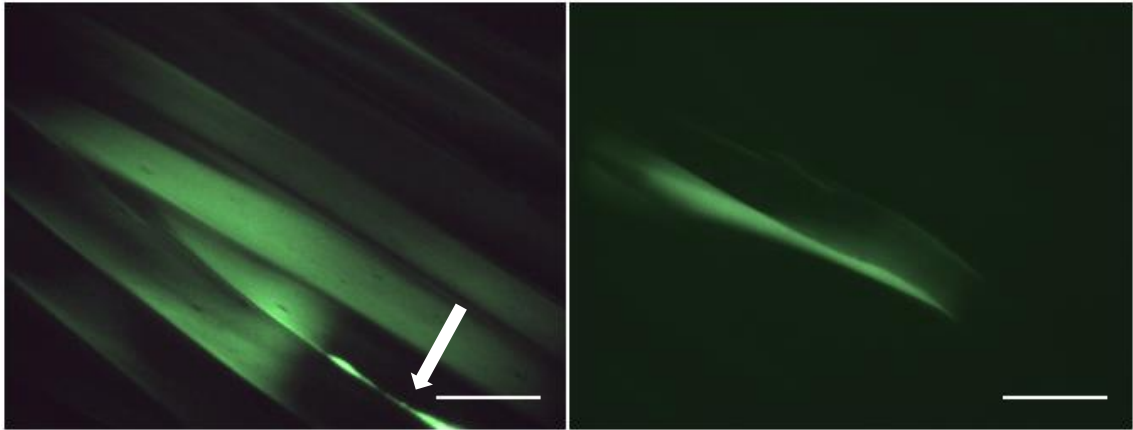
Figure 5.4. *Unclear images of live/dead stained samples. The length of the scale bar is 20 μm.*

As seen in Figure 5.4, it is not clear whether the fluorescent dye has been absorbed by the textile or whether there are cells involved. In the image on the left, the intensity of the fluorescent dye is highest in the gap between two fibers (indicated with an arrow), which could mean that there is a cell under the uppermost fibers. There is also a lot of autofluorescence in the fiber surfaces. In the image on the right, there is not so much autofluorescence, but the fluorescent dye glows from under a single fiber. This could mean, that a cell is growing on the bottom side of that fiber, but the cell cannot be properly seen. Two more unclear images are presented in Figure 5.5.
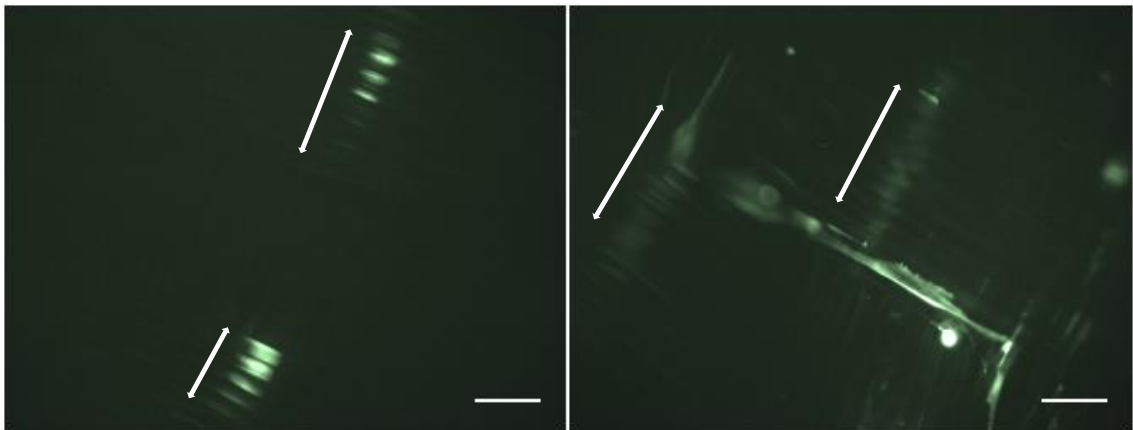
Figure 5.5. *Unclear live/dead images. The length of the scale bar is 50 μm.*

In Figure 5.5, it is be possible that there are cells growing under the fibers as indicated with the white arrows. The situations shown in Figure 5.4 and Figure 5.5 were very common when live/dead imaging was performed. Therefore, live/dead imaging did not give clear results about hiPSC-CMs maturation. Also, only a small amount of cells was found, so it was not reasonable to make comparisons between the cells grown on different textile structures. Instead, the hiPSC-CMs grown on PET textiles were treated as one group in the analysis.

The best method used in this study for evaluating the structural maturation of hiPSC-CMs was immunocytochemistry and imaging of the immunostained samples. Immunostaining revealed the cell structure, sarcomeres and nucleus. Even though the amount of cells detected from immunostained samples was very small, it could be seen that the cells did grow along the PET fibers and their shape became more rod-like. Images of immunostained samples on the different PET textiles are presented in Figure 5.6.
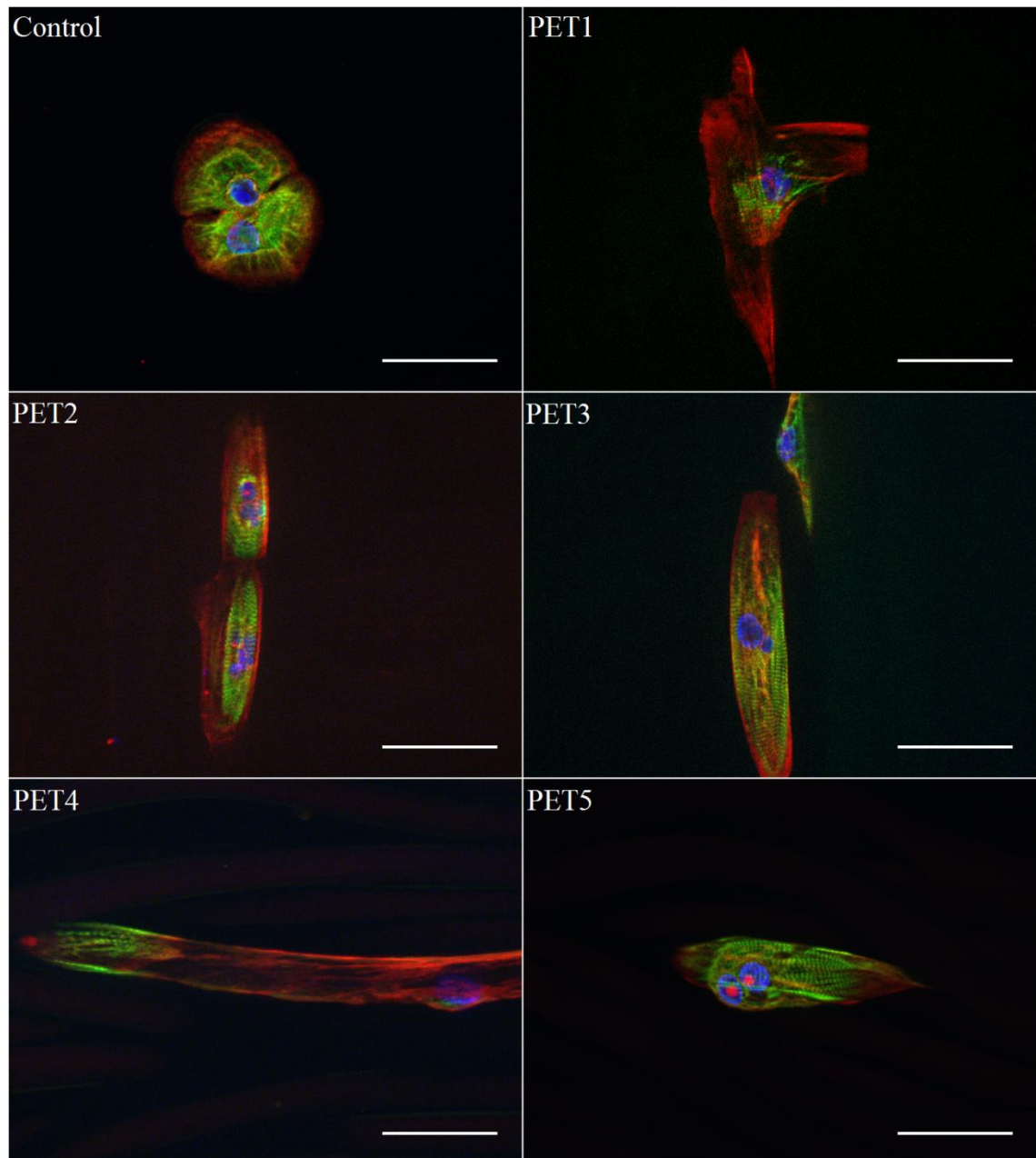
Figure 5.6. Images of immunostained samples. In the image, nucleus is seen in blue (DAPI), MYBPC is seen in green, and troponin T is seen in red. The length of the scale bar is 50 μm. On PET1, the morphology of the cell is different compared to the cells grown on PET2–PET5. This is only because the cell happened to be growing on an interlacing point of the textile. Usually, the cells did not cross interlacing points.

As seen in Figure 5.6, the hiPSC-CMs grown on PET textiles exhibit more adult-like shape than the control cell. Even though the sarcomeres (green) are not well developed in cells grown on PET1 and PET4 in Figure 5.6, it was not a pattern seen in all the cells grown on these particular textiles. Also, the cells did not favor any textile structure over the others, even though in Figure 5.6 the sarcomeres are more developed in cells grown on PET2, PET3 and PET5. All in all, there was a variety of more and less matured cells on all the textile structures.

5.2 Sarcomere Orientation and Length

The sarcomere orientation and length were analyzed with the CytoSpectre software. As a CM matures, its shape changes from circular to rod-like. Along with this transition, the sarcomeres grow in length and align with the longitudinal axis of the CM. (Rodriguez et al. 2014) In this study, it was observed that the hiPSC-CMs were able to grow along the fibers of the PET textiles and become more rod-like in shape. Thus, the hypothesis was, that the mean sarcomere orientation for the cells grown on textiles would be 90°, which is the direction parallel to the longitudinal axis of the fibers. In contrary, the irregularly shaped control cells grown on coverslips had no clear longitudinal direction.

The analysis was performed for 38 hiPSC-CMs grown on PET textiles, and for 35 control hiPSC-CMs grown on coverslips. However, for the cells grown on textiles, only 27 cells remained to analyze, because the signal-to-noise ratio was too low for the rest of the cells. Due to the small amount of cells found on the textiles, the cells grown on different textile structures were not analyzed separately but as one group. The averages of the applicable results from the CytoSpectre analysis are presented in Table 5.1. More detailed results are presented in Appendix C.

Table 5.1. *Results from the CytoSpectre analysis. The values are presented as averages. More detailed results can be found in Appendix C.*

Result	PET	Control
Mean sarcomere orientation	101.87°	48.41°
Circular variance	0.15	0.40
Angular standard deviation	0.51	0.84
Mean sarcomere length	1.91 µm	1.89 µm
Sarcomere length standard deviation	0.23 µm	0.30 µm

Firstly, Table 5.1 shows the mean orientation for cells grown on coverslips and PET textiles. The mean orientation analysis for control cells was not very reasonable since the cells were round and also the sarcomeres were often coiled, as illustrated in Figure 5.7.
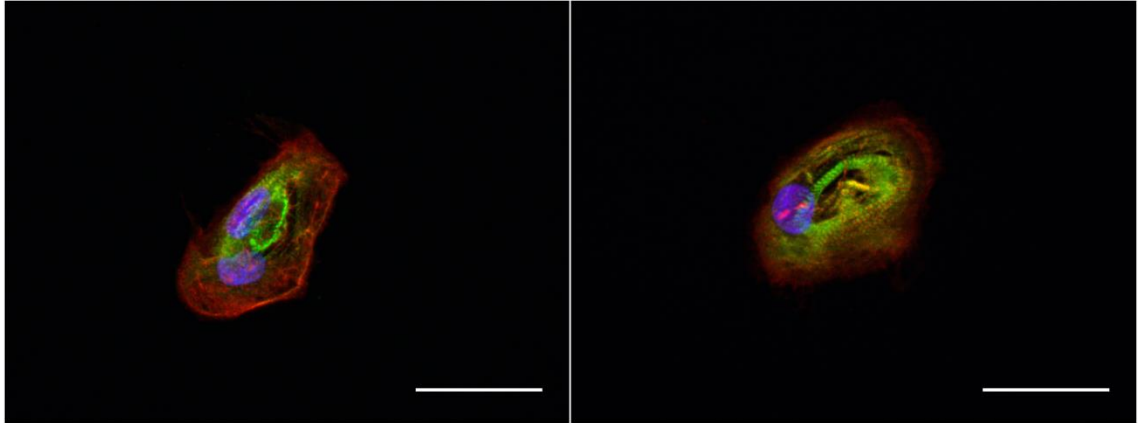
Figure 5.7. *Control hiPSC-CMs grown on coverslips. The length of the scale bar is 50 μm. The cells are circular, and the sarcomere structures are not well organized.*

By contrast, the cells grown on PET textiles showed a rather uniform sarcomere orientation. The hypothesis was that the orientation of the sarcomeres would be 90°, and the average mean orientation was approximately 102°, which is quite close to the hypothesis. Also, two measures for the spread of the orientation distribution are included in Table 5.1: circular variance and angular standard deviation. Indicated by Student's t-test, there was a significant difference in both circular variance ($p = 7.74 \times 10^{-6}$) and angular standard deviation ($p = 2.82 \times 10^{-6}$) when comparing the cells grown on textiles to the cells grown on coverslips. Both of these measures were significantly higher for the hiPSC-CMs cultured on coverslips – for the hiPSC-CMs cultured on PET textiles the values were quite low. The mean orientation distributions of the hiPSC-CMs grown on coverslips (left) and PET textiles (right) are illustrated as rose diagrams in Figure 5.8.
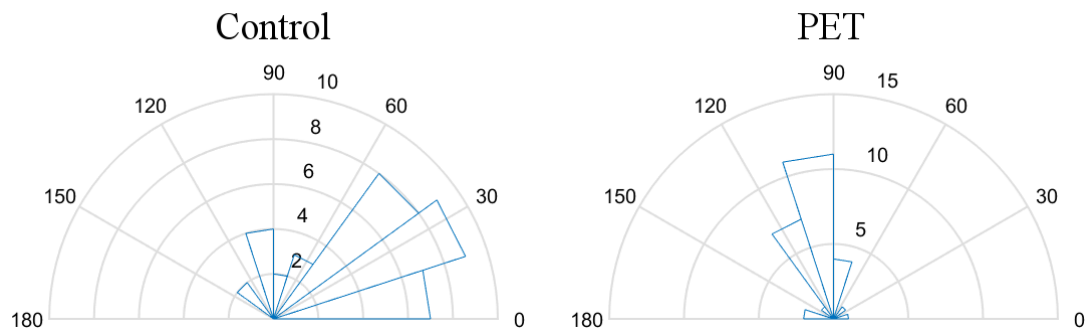
Figure 5.8. *Sarcomere mean orientation distribution of control cells grown on coverslips (left) and cells grown on PET textiles (right). The numbers from the center of circle to the circular arc represent the frequency of the orientations fallen within the sectors – the scales in these two diagrams differ from each other.*

As seen in Figure 5.8, the sarcomere orientations are clearly more uniform for the cells grown on PET textiles. This also correlates with the result, that the sarcomere orientations of the cells grown on textiles got lower circular variance and angular standard deviation values. Also, most of the mean orientations are near to 90° for the cells grown on textiles, which was the orientation parallel to the longitudinal axis of the fibers.

The other analyzed property was the sarcomere length. The reference values for immature hiPSC-CM and adult CM were found in the literature (Yang et al. 2014), and they were 1.6 µm and 2.2 µm, respectively. As seen in Table 5.1, the average sarcomere lengths for cells grown on PET textiles and cells grown on coverslips were 1.91 µm and 1.89 µm, respectively. The values were very close to each other, but the average sarcomere length was slightly longer for the cells grown on textiles. However, as indicated by the Student's t-test, the difference was not statistically significant ($p = 0.64$). For the cells grown on PET textiles, the mean sarcomere lengths varied from 1.60 µm to 2.48 µm (Figure 5.9), and for the cells grown on coverslips, the lengths varied from 1.68 µm to 2.13 µm (Figure 5.10).
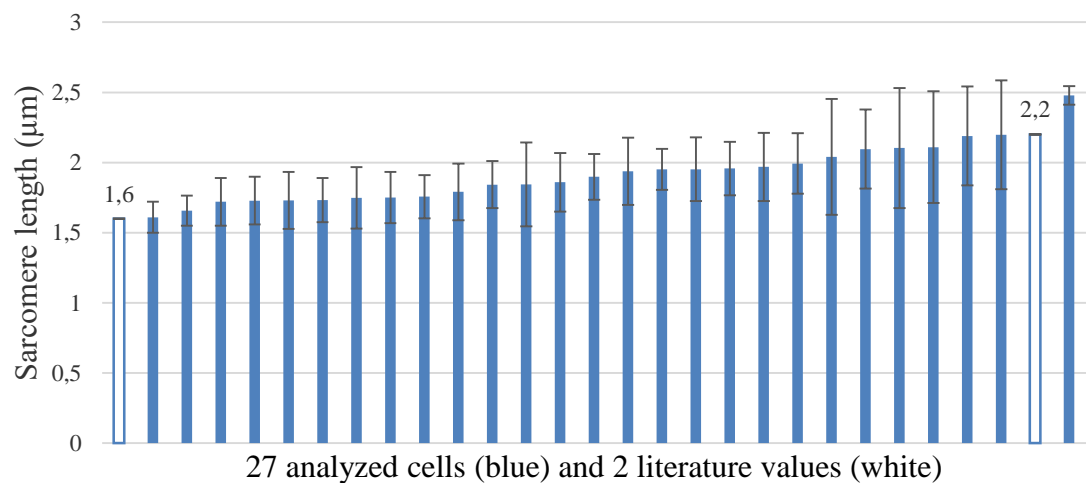
Figure 5.9. Analyzed mean sarcomere lengths for 27 hiPSC-CMs grown on PET (blue bars), and reference values (white bars) given in (Yang et al. 2014). The lengths were organized from the shortest to the longest. The error bars represent the sarcomere length standard deviations.

Figure 5.9 shows the mean sarcomere lengths for all the analyzed hiPSC-CMs grown on PET textiles (27 cells). Almost all the mean sarcomere lengths of cells grown on PET textiles (blue bars) fall in between the literature values (white bars): one value was higher than the literature value for adult cardiomyocytes. Figure 5.10 represents a similar chart for the hiPSC-CMs grown on coverslips.
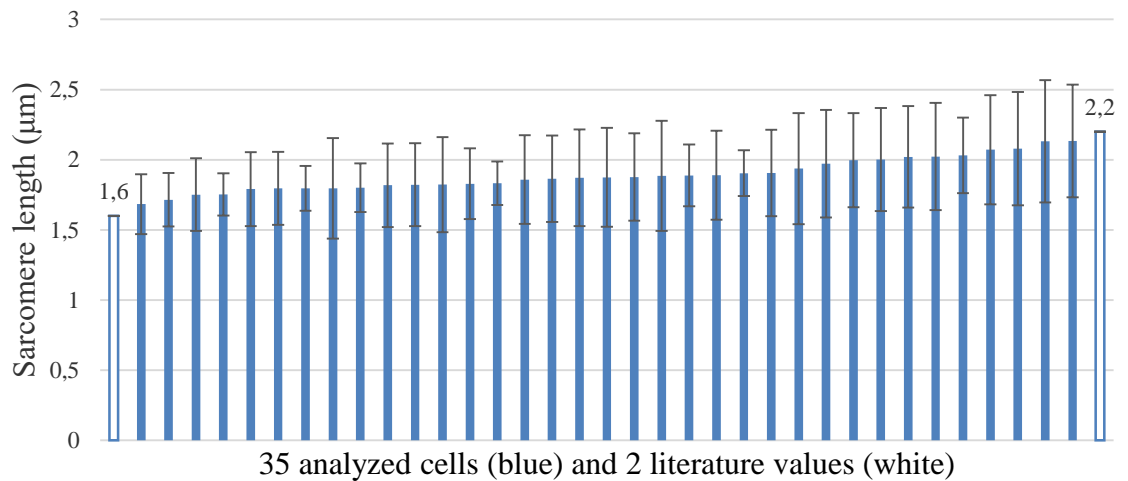
Figure 5.10. *Analyzed mean sarcomere lengths for 35 hiPSC-CMs grown on coverslips (blue bars), and reference values (white bars) given in (Yang et al. 2014). The lengths were organized from the shortest to the longest. The error bars represent the sarcomere length standard deviations.*

As seen in Figure 5.10, all the sarcomere lengths of hiPSC-CMs grown on coverslips (blue bars) fall in between the literature values (white bars). Both in Figure 5.9 and in Figure 5.10 the sarcomere lengths are quite evenly distributed between the lowest and highest values.

In the previous two figures, the error bars represent the sarcomere length standard deviations. As seen in Table 5.1, the average sarcomere length standard deviation for cells grown on PET textiles and cells grown on coverslips were 0.23 μm and 0.30 μm, respectively. The standard deviation of sarcomere lengths was significantly higher ($p = 0.0023$) for the cells grown on coverslips, which means the cells grown on PET textiles exhibited more uniform sarcomere lengths.

5.3 Multinucleation

In addition to other structural factors associated with CM maturation (shape, sarcomere orientation, and sarcomere length), also the multinucleation of the cells was studied. Binucleated hiPSC-CMs were found on PET textiles, and a few of them are shown in Figure 5.11. Binucleated cells were also found on coverslips.
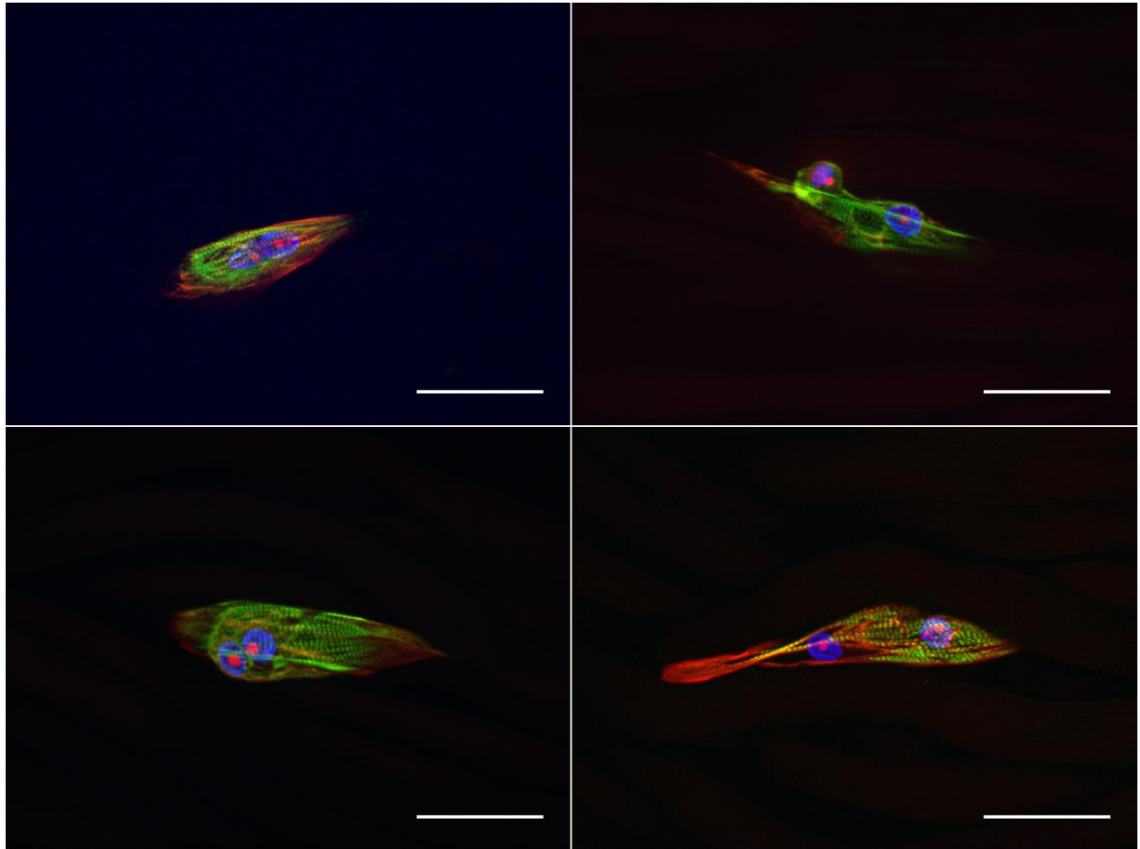
Figure 5.11. *Binucleated hiPSC-CMs on PET textiles. The length of the scale bar is 50 µm. The nuclei are shown in blue (DAPI).*

In Figure 5.11, the nuclei are shown in blue color (DAPI). According to Rodriguez et al. (2014), at the same time as the structural maturation of hiPSC-CMs is occurring, also the percentage of multinucleated cells increases. In this study, approximately 30 % (38 cells analyzed) of hiPSC-CMs grown on PET were binucleated, whereas the percentage for hiPSC-CMs grown on coverslips was approximately 17 % (35 cells analyzed).

6. DISCUSSION

6.1 Maturation of hiPSC-CMs

In this study, the maturation of hiPSC-CMs was evaluated by studying the cells' structural features: shape, sarcomere orientation, sarcomere length, and multinucleation. It was observed, that the hiPSC-CMs grown on PET textiles received topographical cues from the textile structure: the cells grew along the fibers, which made the cells rod-like in shape. In contrary, the hiPSC-CMs grown on coverslips did not receive the same kinds of topographical cues, and they became circular or irregularly shaped.

It has been shown, that the shape of CMs regulate the sarcomere alignment (Bray et al. 2008). For the cells grown in PET textiles, the sarcomeres aligned with the longitudinal axis of the PET fibers. Because the cells grew along the PET fibers, this also meant, that the sarcomeres aligned with the longitudinal axis of the cells. In Figure 6.1, this kind of sarcomere alignment is seen within an immunostained sample. The sarcomeres of control cells were not as well organized. The differences in sarcomere orientation will be discussed next.
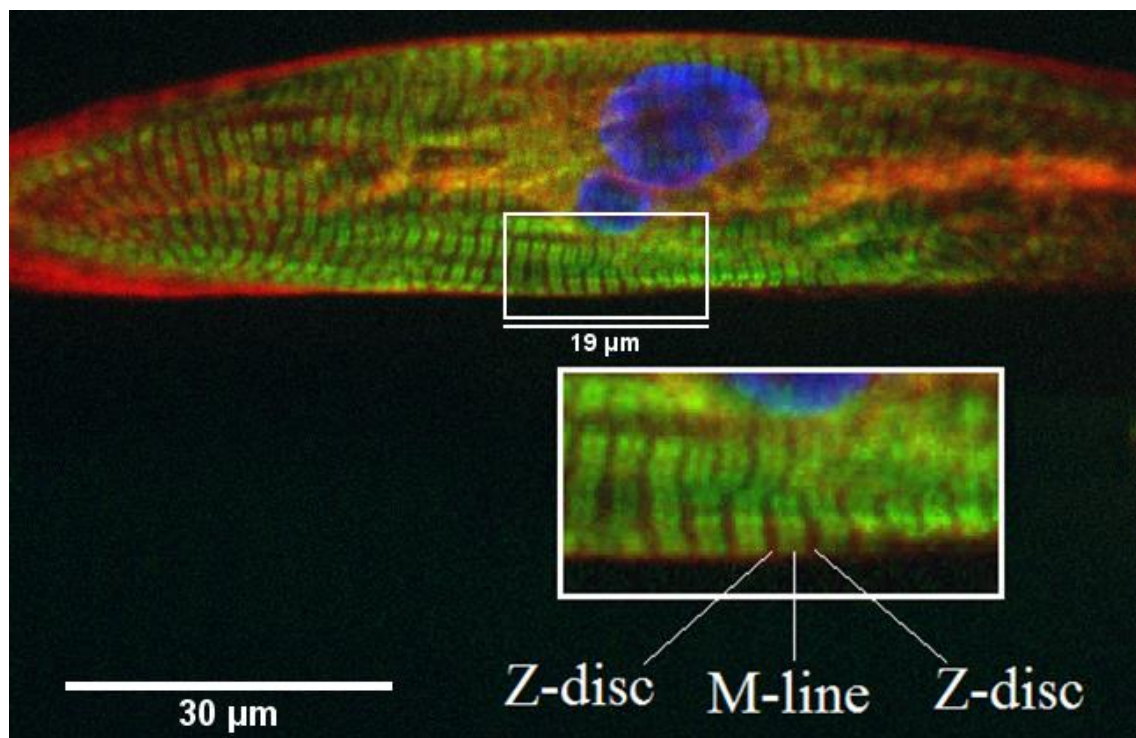
Figure 6.1. *Sarcomere alignment within hiPSC-CMs cultured on PET textile. The sarcomeres are shown in green (MYPBC). The localization of Z-discs and M-lines are also observable.*

The results concerning the sarcomere orientations of the hiPSC-CMs grown on textiles were as expected. The hypothesis was, that the sarcomeres would align parallel to the longitudinal axis of the PET fibers (or cells), which in this case meant the mean orientation should be 90°. The results showed, that the average mean sarcomere orientation for the cells grown on PET textiles was approximately 102°, which is close to the hypothesis. For the cells grown on coverslips the mean orientation analysis was not very reasonable since the cells were round and also the sarcomeres were often coiled. However, the sarcomere orientations of hiPSC-CMs grown on textiles and coverslips could be compared by utilizing measures that describe the spread of the orientation distribution: circular variance and angular standard deviation. Circular variance can get values from 0 to 1, and angular standard deviation from 0 to $\sqrt{2}$. The values of circular variance and angular standard deviation are low when the sarcomeres are aligned along a single orientation, and high when the orientations are evenly spread out around the half circle (0°–180°). The circular variances for cells grown on PET textiles and cells grown on coverslips were 0.15 and 0.40, respectively. In the same order, the angular standard deviations were 0.51 and 0.84. Both of these were significantly lower for the cells grown on textiles, which means that the sarcomeres were more uniformly oriented. Based on these results, it can be concluded, that culturing the hiPSC-CMs on textiles had a desired effect on the sarcomere orientation. In addition to structural maturation, the sarcomere organization is related to the functional maturation of hiPSC-CMs. In a study carried out by Feinberg et al (2012) demonstrated, that improved sarcomeric organization resulted in increased action potential duration, contractile stress and Ca^{2+} transient kinetics, which is consistent with functional maturation.

In the case of sarcomere lengths, there was no significant difference between the cells grown on PET textiles (on average 1.91 μm) and the cells grown on coverslips (on average 1.89 μm). The value was surprisingly good for the control cells, because the literature values for immature hiPSC-CMs and adult CMs were 1.6 μm and 2.2 μm, respectively (Yang et al. 2014). Because the cells grown on coverslips were more immature in shape and the sarcomere orientation was significantly less uniform compared to the cells grown on PET textiles, also the lengths of the sarcomeres were expected to be shorter. Instead, both the cells grown on textiles and the cells grown on coverslips exhibited average sarcomere lengths longer to the ones seen in fetal CMs, which is 1.8 μm (Feric & Radisic 2016). In a study carried out by Lundy et al. (2013), hiPSC-CMs' sarcomere lengths increased to that of fetal CMs by using a long-term culture (80–120 days of *in vitro* differentiation and culture). The cells were grown on coverslips. In this study, the cardiomyocyte differentiation and the culturing of cells on textiles and coverslips took only 27 days, but still the average sarcomere lengths were longer. An explanation for the surprisingly long sarcomeres of the cells grown on coverslips could be that, when coiled (as in Figure 5.7), the sarcomeres become longer on the outer edge than on the inner edge of the circle. This can skew the results.

Not all the sarcomeres were equal in length. For the cells grown on PET textiles, the sarcomere lengths varied from 1.60 μm to 2.48 μm, and for the cells grown on coverslips, the lengths varied from 1.68 μm to 2.13 μm. The maximum sarcomere length is approximately 2.2–2.3 μm, according to various sources (Klabunde 2015; Yang et al. 2014; Kentish et al. 1986; Allen & Kurihara 1982), but the highest mean sarcomere length for hiPSC-CMs cultured on PET textiles was 2.48 μm. This might be an error in the analysis method. The sarcomere lengths were quite evenly distributed between the lowest and the highest values. It seems that, based on the sarcomere lengths, some of the hiPSC-CMs were more mature than others. From the 35 control cells analyzed with CytoSpectre, approximately 77 % of the cells exhibited sarcomere lengths equal or longer to that of fetal CMs. For the cells grown on PET textiles (27 cells were analyzed), the percentage was approximately 63 %. According to Feric & Radisic (2016) the average sarcomere length in a relaxed adult CM is 2.0–2.2 μm. The percentages of control cells and cells grown on PET textiles that exhibited sarcomere lengths longer than 2.0 μm were 23 % and 26 %, respectively. It seems that, even though there was a higher amount of cells that exhibited mean sarcomere lengths typical to immature CMs (1.60–1.79 μm) among the cells grown on textiles than among the control cells, the amount of cells exhibiting sarcomere lengths typical to those of adult CMs was higher for the cells grown on textiles.

The multinucleation of hiPSC-CMs was also studied, even though it is not clear whether the multinucleation of CMs is a maturation marker or not, and the studies regarding this matter are not unanimous. Some claim that hiPSC-CMs are mononucleated whereas most adult CMs are multinucleated (Robertson et al. 2013); some claim that approximately 25 % of adult CMs are multinucleated (Yang et al. 2014); and some claim that fully differentiated CMs only have one nucleus (Sparrow & Schöck 2009). In this study, approximately 30 % of hiPSC-CMs grown on PET were binucleated, whereas the percentage for hiPSC-CMs grown on coverslips was approximately 17 %. Based on these results, it can be argued that growing hiPSC-CMs on PET textiles induces multinucleation. Depending on literature reference, the conclusion could be either desired or undesired. However, taking into consideration the other factors associated with structural maturation of CMs (shape and sarcomere orientation), it is reasonable to argue that cells grown on PET textiles were more mature than the control cells.

6.2 Cell Culture Substrates

Synthetic biomaterials are an attractive option for the production of cell culture substrates, because their properties, including topography and structure, can be tailored for the application. The most frequently used synthetic polymers in the field of cardiac tissue engineering are polyurethane (PU), polylactic acid (PLA), polycaprolactone (PCL), polyglycolic acid (PGA), and their copolymers. (Mathur et al. 2016) All these polymers are (or can be modified to be) biodegradable (Nair & Laurencin 2007). However, the

polymer used in the present study, PET, is not biodegradable but biostable (Ebnesajjad 2013, pp. 94–95)

In tissue engineering it is often desired that the scaffold is biodegradable, because that way the implant introduced to the body in the site of damaged tissue is slowly replaced by regenerated tissue (Nair & Laurencin 2007). Cardiac tissue engineering aims to repair damaged heart tissue, so biodegradable textiles could also be investigated for the studies of improving the maturation of the hiPSC-CMs. The material choice depends on the application and is not always unambiguous: for example, biodegradable PU patches have been investigated for mechanical supports after myocardial infarction, but it is unclear how long the material should remain in place (Hashizume et al. 2013). The biodegradation times alter from polymer to polymer. For example, PGA loses its strength in 1–2 months and mass in 6–12 months, whereas high molecular weight poly-L-lactic acid (PLLA) loses its strength in 6 months and the total resorption *in vivo* takes 2–5.6 years. The degradation rate for PCL is 2–3 years. (Nair & Laurencin 2007)

Also, in tissue engineering, the usual goal is to mimic the mechanical (and other) properties of the native tissue with a biomaterial (van Blitterswijk 2008, pp. 404–405). The Young's modulus of human cardiac muscle is approximately 80 kPa (Herman 2007, p. 214). That is very low compared to the moduli of many biodegradable polymers (for example, 7.0 GPa for PGA; 2.7 GPa for PLLA; and 0.4 GPa for PCL) (Gunatillake & Adhikari 2003). The Young's Modulus of PET is 2.76–4.14 GPa (Callister & Retwisch 2011, p. A9). Also, in the case of textiles, the fibers need to have sufficient strength in order to make the manufacturing of the fabric possible with a weaving loom etc. In order to mimic the mechanical properties of the heart with a textile structure, the textile could be coated with a soft coating thick enough to cover some of the mechanical cues coming from the textile to the cells, but also thin enough to preserve the topographical cues. Hydrogels are a good option for a coating, because their Young's modulus is usually on the order of kiloPascals (Oyen 2014).

PET is a simple, common material, and it was readily available for the present study. PET has been used in cardiac applications before, but, to the writer's knowledge, not for improving the maturation of hiPSC-CMs. In previous studies (Khan et al. 2015; Han et al. 2016; Chun et al. 2015), scaffolds made of aligned or random electrospun nanofibers seemed to be popular, but in the present study, woven textiles were used. Also, the fibers used for making the woven textiles were manufactured by melt spinning process. The fiber diameters used in the previous studies utilizing aligned nanofibers (Khan et al. 2015; Han et al. 2016) varied from 0.7 μm to 0.95 μm. These fiber diameters were very small compared to the fiber diameters of the PET textiles used in this study (20−25 μm). Also, the diameters of the nanofibers were very small compared to the width of adult CMs (10 μm) (Robertson et al. 2013). However, the strategy in these previous studies was a bit different compared to the present study, because the aim was not to grow the cells on top

of single fibers but on top of many aligned fibers guiding the cells' direction of growth along the fiber orientation (illustrated in Figure 2.11, p. 20).

In the previous studies, micropatterning has also been investigated for improving the maturation of hiPSC-CMs. In the study carried out by Rao et al. (2013), the cells were cultured on grooved substrates. The grooves were 10 μm in width, which is also the width of adult CMs (Robertson et al. 2013). By contrast, in the study carried out by Ribeiro et al. (2015) the cells were seeded on polyacrylamide gel patterned with 1 % gelatin lines. The gelatin lines were 20 μm in width, which is close to the fiber diameters of PET textiles used in this study. 20 μm is twice the width of an adult CM (Robertson et al. 2013). In this study, the hiPSC-CMs grew along the PET fibers and also extended their width to the width of the fibers. Because the fibers had a circular cross-section, the cells growing on top of them usually exhibited half circle cross-section. The fiber radius being 10−12.5 μm, the width of the cells can be calculated as $\pi \times r \approx 31\text{--}39$ μm, which is actually huge compared to the values presented by Robertson et al. (2013). In the future, it might be better to use textiles made of thinner fibers (e.g. fiber diameters of 10 μm), so that the width of the cells would better match that of the adult CMs.

In this study, hiPSC-CMs were cultured on five different textiles. The fiber diameters were 20−25 μm for all the textiles, but the textile structures varied. However, the scale of the cells was so small compared to that of the fibers that the cells hardly ever grew across the interlacing points of the textile. In the scale of the cells, the properties of all the textiles were similar, and they did not seem to favor any structure over the others. However, the amount of cells was very small on all the textiles (the possible reasons for that will be discussed in Subchapter 6.3). Some differences between the textile structures could probably have been noticed, if more cells would have attached on the fibers. Imaging-wise a loose structure was more favorable, since, when using brightfield microscopy, more light was able to pass through the textiles. For the cells, a tight structure might be better, so that they would not fall through the textile onto the multiwell plate's bottom when plating the cells. The multiwell plates' bottoms were not studied, but it would have been a good idea to check if the cells were growing there instead of the textiles. That could have also explained why so small amount of cells were found on the textile samples.

6.3 Challenges During the Study

During present study, some challenges emerged, one being that only a very small amount of cells were found on the textiles. There could be many explanations for that. Firstly, there could have been some complications in the dissociation of beating cardiomyocytes. Some of the beating areas collected could have been aspirated during the three dissociation buffer changes. Also, part of the cells might have died during the step where the aggregates were broken down by pressing pipette's tip against the well plate's bottom and pipetting the solution up and down. The step can be quite rough to the CMs, if it is

not done gently enough. Furthermore, maybe there were too small amount of cells used in the dissociation to begin with. The size of the beating aggregates varies enormously, which means the amount of cells within the aggregates varies. Also, the proportion of CMs to the total amount of cells within the aggregates vary.

Secondly, the small amount of cells could be explained by poor cell attachment. If the cells cannot attach on the cell culturing substrate's surface, they get aspirated during medium change. Also, the gelatin coating might have come off, subsequently removing the cells from the PET textile's surface. According to an article, the coating of PET with gelatin is difficult, because the surface of PET lacks functional groups, and many attempts to immobilize gelatin on PET by physical and chemical methods have been done. An approach to a solution that was presented in the article, was an initial surface activation of PET with a dopamine coating, onto which the gelatin coating was added. Dopamine is the synthetic equivalent of particular adhesive protein of mussels, and it is capable of adhering on many different kinds of surfaces including polymers, ceramics, and metals. In the study, gelatin-dopamine-PET samples with covalently immobilized gelatin were obtained. This coating method was developed especially for cardiovascular applications, and it could be applied also to PET textiles. (Giol et al. 2015) Other coatings, such as collagen, could be tested, too. All in all, if the coating coming off the textile was the reason for the small amount of cells, a better coating without compromising the textile topography is needed.

Lastly, the small amount of cells could mean the cells were growing inside the textile structure so that they could not be detected with a microscope. Textiles are three-dimensional (3D) structures, which makes it possible for the cells to "hide" under the fibers. This could be avoided by coating, which forms a film on the textile surface, preventing the cells from penetrating the textile. The coating should be thin enough, so that the textile topography remains unchanged, but also thick enough so that it plugs the routes for cell penetration.

Other challenges that emerged were related to the imaging of the cells grown on textile structures. The textiles were heat treated in order to flatten the structures, but still the 3D nature of the textiles was a challenge when using microscopes. The Zeiss Imager.M2 Axio fluorescence microscope with ApoTome was the best option used in this study, because it allowed the creating of a stack of images, which in turn could be used for the reconstruction of a Z-projection of the image. Z-axis is the one perpendicular to the image plane. Another challenge with imaging was autofluorescence, especially with live/dead imaging. Without staining, the cells could not be detected from the textiles, but also the stainings were not a good answer to the problem, because there was a disturbing amount of autofluorescence. Autofluorescence was also present when imaging the immunostained samples, but the effect was not as disturbing as with live/dead imaging. Actually, sometimes it was even desired to see the 3D structure as well, in order to

understand the locations of the cells within the textiles better. In Figure 6.2, there is a lot of autofluorescence which reveals the PET fibers in addition to the cells.
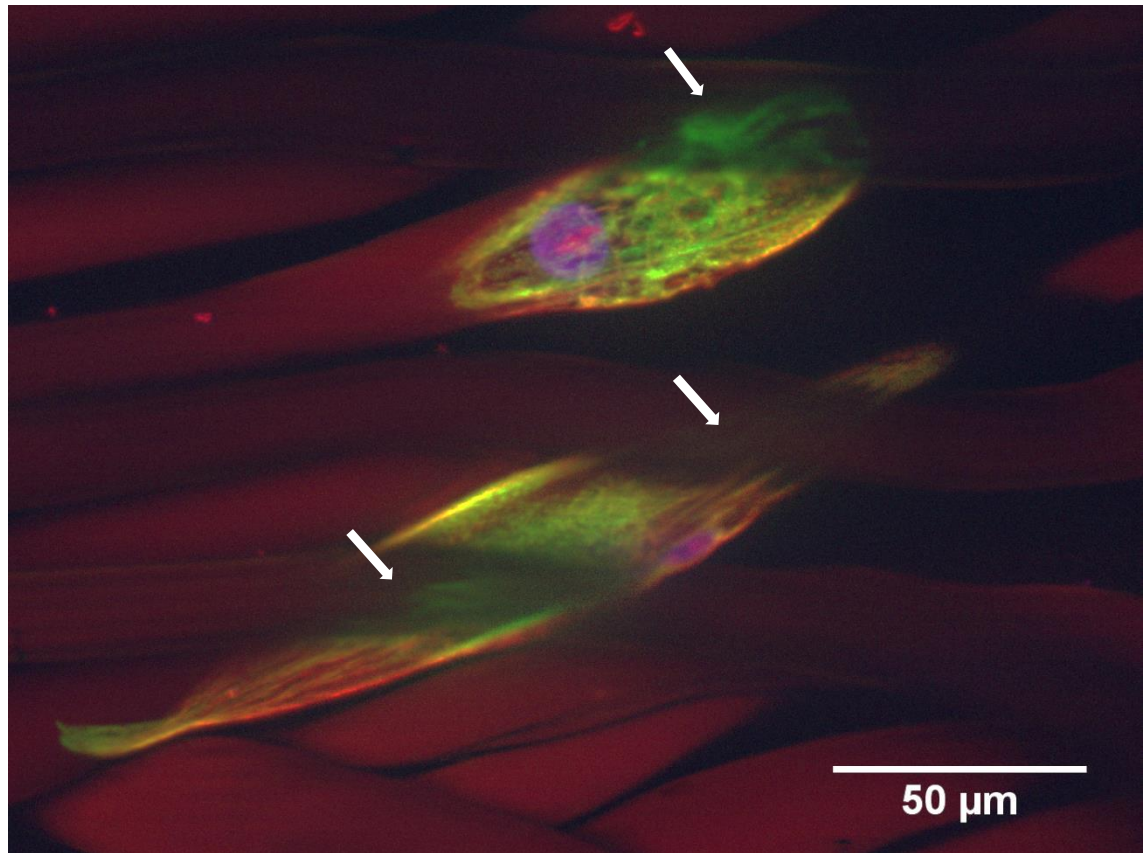
Figure 6.2. hiPSC-CMs growing partly under the PET fibers. In the image, nuclei are seen in blue (DAPI), MYBPC is seen in green, and troponin T is seen in red. The fibers above the cells are indicated with white arrows.

In Figure 6.2, the autofluorescence makes it possible to notice, that three of the PET fibers are above the hiPSC-CMs, as indicated with white arrows. The parts of the three fibers which cross the cells are blurry and mixed with the colors of the cells. Without autofluorescence, these areas might have been just blurry, and the cause of it would have been uncertain.

6.4 Future Studies

In this study, it was demonstrated, that the maturation of hiPSC-CMs was improved by culturing the cells on PET textiles. Using a textile topography, the cells were able to become more rod-like in shape, and also the sarcomere structures became more organized compared to those of hiPSC-CMs grown on flat surfaces. PET probably was not the best material choice, because its surface lacks functional groups, thus making the attachment of the gelatin coating and cells difficult (Giol et al. 2015). In the future, PET textiles could be surface-modified, for example, with plasma treatment (Alagirusamy & Das 2010, p. 452), in order to achieve better attachment of the gelatin coating and cells. Another

option is to use a different material and/or coating. Some suggestions for the future studies were already discussed in Subchapters 6.1–6.3 (textiles made of biodegradable polymers, different coating, and thinner fibers). A few more are introduced in this subchapter.

In the future, it would be useful to study different time points. In this study, the samples were only studied at one time point, at which the hiPSC-CMs had been cultured on the textiles for 11 days (27 days of *in vitro* differentiation and culture). As discussed earlier in Subchapter 6.3, one reason why so small amount of hiPSC-CMs were found on the textiles could be that the gelatin coating was coming off the textile surface simultaneously removing the cells. This effect could be reduced by a shorter culture time. However, a longer culture time would allow the hiPSC-CMs to grow and mature more. A study carried out by Lundy et al. (2013) investigated the effect of long-term culture on the maturation of hiPSC-CMs. The study compared short-term cultured cells (20–40 days of *in vitro* differentiation and culture) to long-term cultured cells (80–120 days). Compared to the short-term cultured cells, the long-term cultured cells exhibited significant improvements in morphology: the cell size and anisotropy increased, the myofibril density and alignment were greater, the sarcomeres were visible by brightfield microscopy and there was a 10-fold increase in the fraction of multinucleated hiPSC-CMs. A longer culturing period could be worth studying with textile structures, too.

Another suggestion for the future is the differentiation of hiPSCs to CMs directly on textile structures. The method has not been very widely studied, but for example Prabhakaran et al. (2014) investigated the differentiation of mouse ESCs to CMs on electrospun poly(D,L-lactide-co-glycolide)/collagen nanofiber substrates (fiber diameters were in the range of 300 ± 65 nm). The study was successful and concluded that the nanofibers provided sufficient chemical and mechanical properties for the ESCs to grow and differentiate into CMs. However, the maturation of the ESC-CMs was not studied. In the method used in this thesis, the cells were differentiated by END-2 method on multiwell plates, from which the beating aggregates were collected, dissociated, and plated on the gelatin coated textiles. In the END-2 method, the hiPSC colonies are plated on top of a mouse endodermal-like (END-2) cell layer. If this differentiation method would be used, also the END-2 cells should be first seeded on the textiles. However, the presence of other cell types is undesired when a certain cell type is being studied. Thus, for differentiating hiPSCs to CMs directly on textiles, some other differentiating method not using other cell types would be better.

7. CONCLUSIONS

The aim of this thesis was to find out whether the structural maturation of hiPSC-CMs can be enhanced by culturing them on woven PET textiles. These cells were compared to hiPSC-CMs grown on coverslips. The studied structural features of the hiPSC-CMs were shape, sarcomere orientation, sarcomere length, and multinucleation.

It was found out that culturing hiPSC-CMs on PET textiles resulted in improved structural maturation of the hiPSC-CMs compared to the hiPSC-CMs grown on coverslips. The cells grew along the PET fibers, which made them rod-like in shape. By analyzing the images taken of the immunostained samples it was found out that, compared to the hiPSC-CMs grown on coverslips, the hiPSC-CMs grown on textiles had significantly more oriented sarcomeres. Also, there were more binucleated cells among the hiPSC-CMs grown on textiles. In contrary, there was no significant difference in the sarcomere lengths. However, based on shape, sarcomere orientation, and multinucleation, it can be argued that the cells grown on textiles were more mature than the cells grown on coverslips.

In this study, there were problems with cell attachment and with cells growing between or under the fibers. Next step for the study would be to find a better coating, which would enhance the cell attachment without compromising the textile topography. In addition, this study focused on the structural maturity, but in the future it would be a good idea to also study the functionality of the hiPSC-CMs grown on PET textiles.

REFERENCES

Acimovic, I., Vilotic, A., Pesl, M., Lacampagne, A., Dvorak, P., Rotrekl, V. & Meli, A.C. (2014). Human Pluripotent Stem Cell-Derived Cardiomyocytes as Research and Therapeutic Tools, BioMed Research International, Vol. 2014(512831), pp. 1-14.

Akovali, G., Banerjee, B., Sen, A.K. & Setua, D.K. (2012). Advances in Polymer Coated Textiles, Smithers Rapra Technology, pp. 157; 161-163.

Alagirusamy, R. & Das, A. (2010). Technical Textile Yarns - Industrial and Medical Applications, Woodhead Publishing, Cambridge, pp. 426; 452-453; 470.

Allen, D.G. & Kurihara, S. (1982). The effects of muscle length on intracellular calcium transients in mammalian cardiac muscle, The Journal of Physiology, Vol. 327, pp. 79-94.

Amit, M., Margulets, V., Segev, H., Shariki, K., Laevsky, I., Coleman, R. & Itskovitz-Eldor, J. (2003). Human feeder layers for human embryonic stem cells, Biology of reproduction, Vol. 68(6), pp. 2150-2156.

Anna, D.H. (ed.). 2011. Occupational Environment - Its Evaluation, Control, and Management. 3rd ed. Virginia, American Industrial Hygiene Association (AIHA), p. 93.

Bers, D.M. (2002). Cardiac excitation–contraction coupling, Nature, Vol. 415(6868), pp. 198-205.

Bilic, J. & Belmonte, J.C.I. (2012). Concise Review: Induced Pluripotent Stem Cells Versus Embryonic Stem Cells: Close Enough or Yet Too Far Apart? Stem Cells, Vol. 30(1), pp. 33-41.

van Blitterswijk, C. (2008). Tissue Engineering, Elsevier, Oxford, pp. 3; 7; 256; 269; 316-317; 328-329; 404-405.

Boretos, J.W. & Eden, M. (1984). Contemporary Biomaterials - Material and Host Response, Clinical Applications, New Technology and Legal Aspects, Noyes Publications, Park Ridge, pp. 232–233.

Boron, W.F. & Boulpaep, E.L. (2005). Medical Physiology: A Cellular And Molecular Approach. Updated ed., Elsevier Saunders, Philadelphia, pp. 232-233; 522.

Bray, M.A., Sheehy, S.P. & Parker, K.K. (2008). Sarcomere Alignment is Regulated by Myocyte Shape, Cell Motility and the Cytoskeleton, Vol. 65(8), pp. 641-651.

Callister, W.D. & Retwisch, D.G. (2011). Materials Science and Engineering, 8th ed., John Wiley & Sons, Asia, p. A9.

Chan, B.P. & Leong, K.W. (2008). Scaffolding in tissue engineering: general approaches and tissue-specific considerations, European Spine Journal, Vol. 17(Suppl 4), pp. 467-479.

Chen, Q., Harding, S.E., Ali, N.N., Lyon, A.R. & Boccaccini, A.R. (2008). Biomaterials in cardiac tissue engineering: Ten years of research survey, Materials Science and Engineering: R: Reports, Vol. 59(1–6), pp. 1-37.

Chun, Y.W., Balikov, D.A., Feaster, T.K., Williams, C.H., Sheng, C.C., Lee, J., Boire, T.C., Neely, M.D., Bellan, L.M., Ess, K.C., Bowman, A.B., Sung, H. & Hong, C.C. (2015). Combinatorial polymer matrices enhance in vitro maturation of human induced pluripotent stem cell-derived cardiomyocytes, Biomaterials, Vol. 67, pp. 52-64.

Dee, K.C., Puleo, D.A. & Bizios, R. (2002). Biomaterials, in: An Introduction to Tissue-Biomaterial Interactions, John Wiley & Sons, Inc., pp. 1-13.

Denning, C., Borgdorff, V., Crutchley, J., Firth, K.S.A., George, V., Kalra, S., Kondrashov, A., Hoang, M.D., Mosqueira, D., Patel, A., Prodanov, L., Rajamohan, D., Skarnes, W.C., Smith, J.G.W. & Young, L.E. (2015). Cardiomyocytes from human pluripotent stem cells: From laboratory curiosity to industrial biomedical platform, Biochimica et Biophysica Acta (BBA) - Molecular Cell Research, pp. 21. Available (accessed 15.3.2016): http://dx.doi.org/10.1016/j.bbamcr.2015.10.014.

Dhandayuthapani, B., Yoshida, Y., Maekawa, T. & Kumar, D.S. (2011). Polymeric Scaffolds in Tissue Engineering Application: A Review, International Journal of Polymer Science, Vol. 2011, pp. 1-19.

Ebersole, G.C., Buettmann, E.G., MacEwan, M.R., Tang, M.E., Frisella, M.M., Matthews, B.D. & Deeken, C.R. (2012). Development of novel electrospun absorbable polycaprolactone (PCL) scaffolds for hernia repair applications, Surgical Endoscopy, Vol. 26(10), pp. 2717-2728.

Ebnesajjad, S. (2013). Handbook of Biopolymers and Biodegradable Plastics - Properties, Processing and Applications, Elsevier, Oxford, pp. 94-95.

Eibl, R., Eibl, D., Pörtner, R., Catapano, G. & Czermak, P. (2009). Cell and Tissue Reaction Engineering, Springer Berlin Heidelberg, pp. 57-59

Feinberg, A.W., Alford, P.W., Jin, H., Ripplinger, C.M., Werdich, A.A., Sheehy, S.P., Grosberg, A. & Parker, K.K. (2012). Controlling the contractile strength of engineered cardiac muscle by hierarchal tissue architecture, Biomaterials, Vol. 33(23), pp. 5732-5741.

Feric, N.T. & Radisic, M. (2016). Maturing human pluripotent stem cell-derived cardiomyocytes in human engineered cardiac tissues, Advanced Drug Delivery Reviews, Vol. 96(1), pp. 110-134.

Giol, E.D., Schaubroeck, D., Kersemans, K., De Vos, F., Van Vlierberghe, S. & Dubruel, P. (2015). Bio-inspired surface modification of PET for cardiovascular applications: Case study of gelatin, Colloids and Surfaces B: Biointerfaces, Vol. 134, pp. 113-121.

Gunatillake, P.A. & Adhikari, R. (2003). Biodegradable synthetic polymers for tissue engineering, European Cells and Materials, Vol. 5, pp. 1-16.

Han, J., Wu, Q., Xia, Y., Wagner, M.B. & Xu, C. (2016). Cell alignment induced by anisotropic electrospun fibrous scaffolds alone has limited effect on cardiomyocyte maturation, Stem Cell Research, Vol. 16(3), pp. 740-750.

Hashizume, R., Hong, Y., Takanari, K., Fujimoto, K.L., Tobita, K. & Wagner, W.R. (2013). The effect of polymer degradation time on functional outcomes of temporary elastic patch support in ischemic cardiomyopathy, Biomaterials, Vol. 34(30), pp. 7353-7363.

Herman, I.P. (2007). Physics of the Human Body, 1st ed., Springer Berlin Heidelberg, Germany, p. 214.

Hu, X. & Yang, H.H. (2000). 1.11 - Polyamide and Polyester Fibers, in: Zweben, A.K. (ed.), Comprehensive Composite Materials, Pergamon, Oxford, pp. 327-344.

Karamuk, E., Mayer, J., Wintermantel, E. & Akaike, T. (1999). Partially Degradable Film/Fabric Composites: Textile Scaffolds for Liver Cell Culture, Artificial Organs, Vol. 23(9), pp. 881-884.

Kartasalo, K., Pölönen, R., Ojala, M., Rasku, J., Lekkala, J., Aalto-Setälä, K. & Kallio, P. (2015). CytoSpectre: a tool for spectral analysis of oriented structures on cellular and subcellular levels, BMC Bio informat ics, Vol. 16(344), pp. 1-23.

Kentish, J.C., ter Keus, H.E.D.J., Ricciardi, L., Bucx, J.J.J. & Noble, M.I.M. (1986). Comparison between the Sarcomere Length-Force Relations of Intact and Skinned Trabeculae from Rat Right Ventricle: Influence of Calcium Concentrations on These Relations, Circulation Research, Vol. 58(6), pp. 755-768.

Khan, J.M., Lyon, A.R. & Harding, S.E. (2013). The case for induced pluripotent stem cell-derived cardiomyocytes in pharmacological screening, British Journal of Pharmacology, Vol. 169(2), pp. 304-317.

Khan, M., Xu, Y., Hua, S., Johnson, J., Belevych, A., Janssen, P.M.L., Gyorke, S., Guan, J. & Angelos, M.G. (2015). Evaluation of Changes in Morphology and Function of

Human Induced Pluripotent Stem Cell Derived Cardiomyocytes (HiPSC-CMs) Cultured on an Aligned-Nanofiber Cardiac Patch. PLoS One, Vol. 10(5), pp. 1-19.

Klabunde, R.E. (2015). Length-Tension Relationship for Cardiac Muscle (Effects of Preload), Cardiovascular Physiology Concepts, pp. 1.3.2016. Available (accessed 1.3.2016): http://www.cvphysiology.com/Cardiac%20Function/CF004.htm.

Kujala, V., Pekkanen-Mattila, M. & Aalto-Setälä, K. (2011). Human Pluripotent Stem Cell-Derived Cardiomyocytes: Maturity and Electrophysiology, in: Kallos, M.S. (ed.), Embryonic Stem Cells - Differentiation and Pluripotent Alternatives, InTech, pp 185-204.

Kurosawa, H. (2007). Methods for inducing embryoid body formation: in vitro differentiation system of embryonic stem cells, Journal of Bioscience and Bioengineering, Vol. 103(5), pp. 389-398.

van Laake, L.W., Passier, R., Monshouwer-Kloots, J., Verkleij, A.J., Lips, D.J., Freund, C., den Ouden, K., Ward-van Oostwaard, D., Korving, J., Tertoolen, L.G., van Echteld, C.J., Doevendans, P.A. & Mummery, C.L. (2007). Human embryonic stem cell-derived cardiomyocytes survive and mature in the mouse heart and transiently improve function after myocardial infarction, Stem Cell Research, Vol. 1(1), pp. 9-24.

de Lázaro, I., Yilmazer, A. & Kostarelos, K. (2014). Induced pluripotent stem (iPS) cells: A new source for cell-based therapeutics? Journal of Controlled Release, Vol. 185(2014), pp. 37-44.

Lundy, S.D., Zhu, W.Z., Regnier, M. & Laflamme, M.A. (2013). Structural and Functional Maturation of Cardiomyocytes Derived from Human Pluripotent Stem Cells, Stem Cells and Development, Vol. 22(14), pp. 1991-2002.

Maron, B.J. & Maron, M.S. (2013). Hypertrophic cardiomyopathy, The Lancet, Vol. 381(9862), pp. 242-255.

Mather, R.R. & Wardman, R.H. (2011). Chemistry of Textile Fibres, Royal Society of Chemistry, Cambridge, pp. 130-131.

Mathur, A., Ma, Z., Loskill, P., Jeeawoody, S. & Healy, K.E. (2016). In vitro cardiac tissue models: Current status and future prospects, Advanced Drug Delivery Reviews, Vol. 96(1), pp. 203-213.

Matthews, G.G. (2009). Cellular Physiology of Nerve and Muscle, Wiley-Blackwell, Hoboken, NJ, USA, pp. 191-193.

McCain, M.L., Agarwal, A., Nesmith, H.W., Nesmith, A.P. & Parker, K.K. (2014). Micromolded gelatin hydrogels for extended culture of engineered cardiac tissues, Biomaterials, Vol. 35(21), pp. 5462-5471.

McKeen, L.W. (2010). Fatigue and Tribological Properties of Plastics and Elastomers, 2nd ed., Elsevier, USA, p. 100.

Michler, G.H. & Baltá-Calleja, F.J. (2012). Nano- and Micromechanics of Polymers - Structure Modification and Improvement of Properties, Hanser Publishers, München, p. 270.

Moreno, M.J., Ajji, A., Mohebbi-Kalhori, D., Rukhlova, M., Hadjizadeh, A. & Bureau, M.N. (2011). Development of a compliant and cytocompatible micro-fibrous polyethylene terephthalate vascular scaffold, Journal of Biomedical Materials Research, Vol. 97B(2), pp. 201-214.

Mummery, C.L., Zhang, J., Ng, E.S., Elliott, D.A., Elefanty, A.G. & Kamp, T.J. (2012). Differentiation of Human ES and iPS Cells to Cardiomyocytes: A Methods Overview, Circulation Research, Vol. 111(3), pp. 344-358.

Mummery, C., Ward-Van Oostwaard, D., Doevendans, P., Spijker, R., Van Den Brink, S., Hassink, R., Van Der Heyden, M., Opthof, T., Pera, M., De La Riviere, A.B., Passier, R. & Tertoolen, L. (2003). Differentiation of human embryonic stem cells to cardiomyocytes: role of coculture with visceral endoderm-like cells, Circulation, Vol. 107(21), pp. 2733-2740.

Nair, L.S. & Laurencin, C.T. (2007). Biodegradable polymers as biomaterials, Progress in Polymer Science, Vol. 32(8–9), pp. 762-798.

O'Brien, F.J. (2011). Biomaterials & scaffolds for tissue engineering, Materials Today, Vol. 14(3), pp. 88-95.

Oyen, M.L. (2014). Mechanical characterisation of hydrogel materials, International Materials Reviews, Vol. 59(1), pp. 44-59.

Pasqualini, F.S., Sheehy, S.P., Agarwal, A., Aratyn-Schaus, Y. & Parker, K.K. (2015). Structural Phenotyping of Stem Cell-Derived Cardiomyocytes, Stem Cell Reports, Vol. 4(3), pp. 340-347.

Passier, R., Oostwaard, D.W., Snapper, J., Kloots, J., Hassink, R.J., Kuijk, E., Roelen, B., De La Riviere, A.B. & Mummery, C. (2005). Increased cardiomyocyte differentiation from human embryonic stem cells in serum-free cultures, Stem Cells, Vol. 23(6), pp. 772-780.

Patel, N.R. & Gohil, P.P. (2012). A Review on Biomaterials: Scope, Applications & Human Anatomy Significance, International Journal of Emerging Technology and Advanced Engineering, Vol. 2(4), pp. 91-101.

Prabhakaran, M.P., Mobarakeh, L.G., Kai, D., Karbalaie, K., Nasr-Esfahani, M.H. & Ramakrishna, S. (2014). Differentiation of embryonic stem cells to cardiomyocytes on electrospun nanofibrous substrates, Journal of Biomedical Materials Research Part B: Applied Biomaterials, Vol. 102(3), pp. 447-454.

Rao, C., Prodromakis, T., Kolker, L., Chaudhry, U.A.R., Trantidou, T., Sridhar, A., Weekes, C., Camelliti, P., Harding, S.E., Darzi, A., Yacoub, M.H., Athanasiou, T. & Terracciano, C.M. (2013). The effect of microgrooved culture substrates on calcium cycling of cardiac myocytes derived from human induced pluripotent stem cells, Biomaterials, Vol. 34(10), pp. 2399-2411.

Ratner, B.D., Hoffman, A.S., Schoen, F.J. & Lemons, J.E. (ed.). 2013. Biomaterials Science - An Introduction to Materials in Medicine. 3rd ed. Canada, Academic Press, pp. 408-409; 700.

Ribeiro, M.C., Tertoolen, L.G., Guadix, J.A., Bellin, M., Kosmidis, G., D'Aniello, C., Monshouwer-Kloots, J., Goumans, M., Wang, Y., Feinberg, A.W., Mummery, C.L. & Passier, R. (2015). Functional maturation of human pluripotent stem cell derived cardiomyocytes in vitro – Correlation between contraction force and electrophysiology, Biomaterials, Vol. 51(1), pp. 138-150.

Robertson, C., Tran, D.D. & George, S.C. (2013). Concise Review: Maturation Phases of Human Pluripotent Stem Cell-Derived Cardiomyocytes, Stem cells, Vol. 31(5), pp. 829-837.

Rodriguez, M.L., Graham, B.T., Pabon, L.M., Han, S.J., Murry, C.E. & Sniadecki, N.J. (2014). Measuring the Contractile Forces of Human Induced Pluripotent Stem Cell-Derived Cardiomyocytes With Arrays of Microposts, Journal of Biomechanical Engineering, Vol. 136(5), pp. 0510051-05100510.

Salick, M.R., Napiwocki, B.N., Sha, J., Knight, G.T., Chindhy, S.A., Kamp, T.J., Ashton, R.S. & Crone, W.C. (2014). Micropattern width dependent sarcomere development in human ESC-derived cardiomyocytes, Biomaterials, Vol. 35(15), pp. 4454-4464.

Schmidt, R.F. & Thews, G. (ed.). 2013. Human Physiology. Germany, Springer Science & Business Media. p. 360.

Severs, N.J. (2000). The cardiac muscle cell, Bioessays, Vol. 22(2), pp. 188-199.

Sparrow, J.C. & Schöck, F. (2009). The initial steps of myofibril assembly: integrins pave the way, Nature Reviews Molecular Cell Biology, Vol. 10(4), pp. 293-298.

Stenlund, K. (2013). Fabrication and Properties of Woven Structures for Biomedical Applications, Master's Thesis, Tampere University of Technology, Tampere, 86 p.

Takahashi, K., Tanabe, K., Ohnuki, M., Narita, M., Ichisaka, T., Tomoda, K. & Yamanaka, S. (2007). Induction of Pluripotent Stem Cells from Adult Human Fibroblasts by Defined Factors, Cell, Vol. 131(5), pp. 861-872.

Takahashi, K. & Yamanaka, S. (2006). Induction of Pluripotent Stem Cells from Mouse Embryonic and Adult Fibroblast Cultures by Defined Factors, Cell, Vol. 126(4), pp. 663-676.

Tamayol, A., Akbari, M., Annabi, N., Paul, A., Khademhosseini, A. & Juncker, D. (2013). Fiber-based tissue engineering: Progress, challenges, and opportunities, Biotechnology Advances, Vol. 31(5), pp. 669-687.

Tao, X. (ed.). 2001. Smart Fibres, Fabrics and Clothing. Cambridge, Woodhead Publishing. pp. 298; 300; 304.

de Tombe, P.P. (2003). Cardiac myofilaments: mechanics and regulation, Journal of Biomechanics, Vol. 36(5), pp. 721-730.

Tzatzalos, E., Abilez, O.J., Shukla, P. & Wu, J.C. (2016). Engineered heart tissues and induced pluripotent stem cells: Macro- and microstructures for disease modeling, drug screening, and translational studies, Advanced Drug Delivery Reviews, Vol. 96, pp. 234-244.

Vunjak-Novakovic, G., Tandon, N., Godier, A., Maidhof, R., Marsano, A., Martens, T.P. & Radisic, M. (2010). Challenges in Cardiac Tissue Engineering, Tissue Engineering Part B: Reviews, Vol. 16(2), pp. 169-187.

Wang, P., Yu, J., Lin, J. & Tsai, W. (2011). Modulation of alignment, elongation and contraction of cardiomyocytes through a combination of nanotopography and rigidity of substrates, Acta Biomaterialia, Vol. 7(9), pp. 3285-3293.

Williams, D.F. (1999). Williams Dictionary of Biomaterials, Liverpool University Press, Liverpool, pp. 40-44.

World Health Organization (2015). Cardiovascular diseases (CVDs), pp. 26.11.2015. http://www.who.int/mediacentre/factsheets/fs317/en/.

Wulfhorst, B., Gries, T. & Veit, D. (2006). Textile Technology, Hanser Publishers, Munich, p. 134.

Yamanaka, S. (2012). Induced Pluripotent Stem Cells: Past, Present, and Future, Cell Stem Cell, Vol. 10(6), pp. 678-684.

Yang, X., Pabon, L. & Murry, C.E. (2014). Engineering Adolescence: Maturation of Human Pluripotent Stem Cell–Derived Cardiomyocytes, Circulation Research, Vol. 114(3), pp. 511-523.

Yu, J., Vodyanik, M.A., Smuga-Otto, K., Antosiewicz-Bourget, J., Frane, J.L., Tian, S., Nie, J., Jonsdottir, G.A., Ruotti, V., Stewart, R., Slukvin, I.I. & Thomson, J.A. (2007). Induced pluripotent stem cell lines derived from human somatic cells, Science, Vol. 318(5858), pp. 1917-1920.

Zhang, D., Shadrin, I.Y., Lam, J., Xian, H., Snodgrass, H.R. & Bursac, N. (2013). Tissue-engineered cardiac patch for advanced functional maturation of human ESC-derived cardiomyocytes, Biomaterials, Vol. 34(23), pp. 5813-5820.

Zong, X., Bien, H., Chung, C., Yin, L., Fang, D., Hsiao, B.S., Chu, B. & Entcheva, E. (2005). Electrospun fine-textured scaffolds for heart tissue constructs, Biomaterials, Vol. 26(26), pp. 5330-5338.

APPENDIX A: DISSOCIATION BUFFERS

Table 1. Contents of the dissociation buffer1 (Low-Ca), pH 6.9.

Volume	Ingredient	Quantity
12 ml	NaCl	1 M
0.54 ml	KCl	1 M
0.5 ml	$MgSO_4$	1 M
0.5 ml	Na pyruvate	1 M
2 ml	Glucose	1 M
20 ml	Taurine	0.1 M
1 ml	HEPES	1 M
	pH correction (NaOH)	

Table 2. Contents of the dissociation buffer 2 (Enzyme medium), pH 6.9.

Volume	Ingredient	Quantity
12 ml	NaCl	1 M
3 µl	CaCl2	1 M
0.54 ml	KCl	1 M
0.5 ml	$MgSO_4$	1 M
0.5 ml	Na pyruvate	1 M
2 ml	Glucose	1 M
20 ml	Taurine	0.1 M
1 mg/ml	Collagenase A	
1 ml	HEPES	1 M
	pH correction (NaOH)	

Table 3. *Contents of the dissociation buffer 3 (KB medium), pH 7.2.*

Volume	Ingredient	Quantity
3 ml	K_2HPO_4	1 M
8.5 ml	KCl	1 M
2 mmol/L	Na_2ATP	
0.5 ml	$MgSO_4$	1 M
0.1 ml	EGTA	1 M
0.5 ml	Na pyruvate	1 M
2 ml	Glucose	1 M
5 ml	Creatine	0.1 M
20 ml	Taurine	0.1 M

APPENDIX B: DOUBLE-FLUORESCENCE PROTOCOL

Double-Fluorescence protocol   **Date:_____**

Samples: _____

☐   **WASH 2 * 5 min** PBS (1 ml, 0.01 M, pH 7.4)

☐   **FIXING 4% PFA 20 min** (0.7 ml)

☐   **WASH 2 * 5 min** PBS (1 ml, 0.01 M, pH 7.4) LEAVE in PBS!

☐   **BLOCKING: 10% NDS, 0.1% TritonX-100, 1% BSA in PBS 45 min RT**

☐   **WASH: 1% NDS, 0.1% TritonX-100, 1% BSA in PBS**

☐   **MIXTURE OF PRIMARIES: 1% NDS, 0.1% TritonX-100, 1% BSA in PBS in +4 C ON**
(24 kuoppalevy: 150 µl primaari/kuoppa)

Well	ANTIBODY	DILUTION	ORIGIN
I	_____	_____	_____
II	_____	_____	_____
III	_____	_____	_____
I	_____	_____	_____
II	_____	_____	_____
III	_____	_____	_____
I	_____	_____	_____
II	_____	_____	_____
I	_____	_____	_____
II	_____	_____	_____
I	_____	_____	_____
II	_____	_____	_____
I	_____	_____	_____
II	_____	_____	_____
I	_____	_____	_____
II	_____	_____	_____
I	_____	_____	_____
II	_____	_____	_____
I	_____	_____	_____
II	_____	_____	_____
I	_____	_____	_____
II	_____	_____	_____

☐ **WASH: 3 * 5-7 min 1% BSA in PBS**

☐ **MIXTURE OF SECONDARIES: 1% BSA in PBS 1 h RT**

Well	ANTIBODY	DILUTION	ORIGIN
I	_____	_____	_____
II	_____	_____	_____
III	_____	_____	_____
I	_____	_____	_____
II	_____	_____	_____
III	_____	_____	_____
I	_____	_____	_____
II	_____	_____	_____
I	_____	_____	_____
II	_____	_____	_____
I	_____	_____	_____
II	_____	_____	_____
I	_____	_____	_____
II	_____	_____	_____
I	_____	_____	_____
II	_____	_____	_____
I	_____	_____	_____
II	_____	_____	_____
I	_____	_____	_____
II	_____	_____	_____
I	_____	_____	_____
II	_____	_____	_____

☐ **WASH 3 *5 min in PBS**

☐ **WASH 2 * 5 min in PB**

☐ **Dry and mount with Vectashield + coverslips**

☐ **Store +4C light protected**

Stainings: ☐ OK ☐ NOT OK **Initials:** _____
Make comments about the staining in back of this paper if not good!!!!
Store the original sheets in

APPENDIX C: CYTOSPECTRE RESULTS

Table 1. *Results from the CytoSpectre analysis: hiPSC-CMs grown on PET. 27 cells were analyzed.*

Mean orientation (°)	Angular std (°)	Mean wavelength = sarcomere length (µm)	Std wavelength(µm)
111.24	0.61	2.04	0.41
93.34	0.57	1.90	0.16
92.75	0.69	1.94	0.24
123.31	0.29	2.19	0.35
177.97	0.70	2.10	0.43
99.53	0.59	1.66	0.11
123.21	0.30	1.86	0.21
114.04	0.61	1.73	0.16
121.85	0.68	2.10	0.28
52.13	0.17	1.79	0.20
91.92	0.62	1.75	0.18
108.22	0.40	1.84	0.30
95.18	0.82	1.84	0.17
132.82	0.19	1.73	0.20
93.56	0.68	1.73	0.17
85.67	0.56	1.76	0.15
86.52	0.67	1.96	0.19
93.48	0.25	1.61	0.11
95.50	0.52	1.95	0.15
171.58	0.30	2.11	0.40
1.32	0.47	2.20	0.39
105.53	0.04	2.48	0.07
76.43	0.48	1.75	0.22
106.78	0.69	1.99	0.22
100.99	0.55	1.95	0.23
110.64	0.71	1.97	0.24
84.98	0.49	1.72	0.17
Average = 101.87	Average = 0.51	Average = 1.91	Average = 0.23

Table 2. *Results from the CytoSpectre analysis: control hiPSC-CMs grown on coverslips. 35 cells were analyzed.*

Mean orientation (°)	Angular std (°)	Mean wavelength = sarcomere length (µm)	Std wavelength (µm)
43.66	0.37	2.13	0.44
96.81	0.59	1.90	0.16
26.92	0.72	1.91	0.31
51.42	0.74	1.97	0.38
38.25	0.69	1.80	0.26
26.38	1.08	1.88	0.35
53.43	0.71	2.00	0.33
41.06	1.14	2.02	0.38
13.32	1.24	1.89	0.39
59.20	0.67	1.80	0.16
23.63	1.25	1.86	0.31
9.15	1.25	1.82	0.30
31.62	0.59	1.82	0.30
90.67	0.52	1.71	0.19
139.73	1.38	1.94	0.40
85.52	0.50	1.75	0.15
27.67	1.36	1.80	0.36
58.10	0.65	1.68	0.21
48.48	1.21	1.88	0.31
23.68	0.84	1.86	0.32
49.56	0.26	2.00	0.37
64.08	0.75	2.03	0.27
27.43	0.76	1.79	0.26
34.21	1.15	1.82	0.34
39.47	0.68	1.75	0.26
83.13	0.68	1.83	0.16
10.14	1.32	1.89	0.32
11.64	0.66	1.80	0.17
22.70	0.95	1.87	0.34
97.07	0.68	1.89	0.22
6.68	1.04	2.13	0.40
96.66	0.75	1.83	0.25
8.90	0.54	2.08	0.40
13.89	0.50	2.02	0.36
140.20	1.31	2.07	0.39
Average = 48.41	Average = 0.84	Average = 1.89	Average = 0.30

APPENDIX D: REAGENTS AND THEIR SUPPLIERS AND/OR MANUFACTURERS

Table 1. *List of used reagents and their suppliers and/or manufacturers which were not mentioned in Chapter 4.*

Reagent/Product	Supplier/Manufacturer
2-mercaptoethanol	Life Technologies
ascorbic acid	Sigma
bovine serum albumin (BSA)	Sigma-Aldrich
fetal bovine serum (FBS)	Immunodiagnostic, Biosera
Glutamax	Life Technologies
KO-DMEM	Life Technologies
KO-SR	Life Technologies
Mitomycin C	R&D Systems Bio-Techne, Tocris
Non-Essential Amino Acids (NEAA)	Life Technologies
normal donkey serum (NDS)	Merck Millipore
paraformaldehyde (PFA)	Sigma-Aldrich
Penicillin/Streptomycin (Pen/Strep)	City-Lab, Lonza
phosphate buffered saline (PBS)	Life Technologies, Lonza
TritonX-100	Sigma Aldrich